THE GEOLOGICAL SOCIETY OF AMERICA®

Timing and thermal evolution of fold-and-thrust belt formation in the Ultima Esperanza District, 51°S Chile: Constraints from K-Ar dating and illite characterization

Annette Süssenberger[1,†], Susanne T. Schmidt[1,†], Klaus Wemmer[2,†], Lukas P. Baumgartner[3,†], and Bernard Grobéty[4,†]
[1]*Department of Earth Sciences, University of Geneva, 13 Rue des Maraîchers, 1205 Geneva, Switzerland*
[2]*Geoscience Center, University of Göttingen, Goldschmidtstraße 3, 37077 Göttingen, Germany*
[3]*Institute of Earth Sciences, University of Lausanne, 1015 Lausanne, Switzerland*
[4]*Department of Geosciences, University of Fribourg, Chemin du Musée, 1700 Fribourg, Switzerland*

ABSTRACT

K-Ar dating on synkinematically formed illite in low-grade metamorphic pelites was used to set new time constraints on the development of the Patagonian retroarc fold-and-thrust belt caused by the subduction of the Antarctic plate beneath the South American plate. The combined use of illite crystallinity (Kübler index), polytype quantification, and K-Ar dating of illite fractions (<0.2, <2, and 2–6 µm) is a powerful tool in constraining the missing time gap between the emergent fold-and-thrust belt formation and early Miocene uplift of the Magallanes Basin. Four distinct periods of illite growth were identified based on their K-Ar ages and degree of regional metamorphism: (1) early Cenomanian (98 Ma) illite crystallization, (2) widespread early Campanian (ca. 80 Ma) long-lasting burial illitization processes under anchizonal metamorphic conditions, (3) a significant period of illite formation in the early Paleocene (ca. 60 Ma), and (4) a late stage of illite growth in the early Eocene (55–46 Ma) under epizonal conditions. Based on K-Ar fine fraction ages and Kübler index values, we propose to subdivide the internal domain along the Río Nutria and Río Rincon thrust into a thrust zone with maximum rock uplift in the west and a foreland-vergent imbricate thrust zone in the east.

The earliest indication for the emergent fold-and-thrust belt formation in the hinterland is documented in a metapelitic clast (sample 14-9, <2 µm) within the Upper Cretaceous Cerro Toro conglomerate, which yielded a K-Ar cooling age of 98.3 ± 1.2 Ma and an epizonal Kübler index value of 0.24 Δ°2Θ. After a certain period of geological quiescence, an interval of major thrusting and rock uplift occurred between ca. 60 and 46 Ma. The west-dipping Río Nutria and Río Rincon thrusts record the onset of fold-and-thrust belt activity, which can be placed close to 60 Ma. In the western part of the internal domain, thrusts remained active, and associated structural uplift is recorded until 46 Ma by K-Ar illite cooling ages. Flexural subsidence driven by thrust sheet loading in the internal domain was responsible for the eastward migration of the foreland depocenter and a rapid increase in sedimentation rate along the monoclinal belt.

Our results prove a synchronous onset of thick-skinned thrusting between 49°S and 55°S and suggest constant convergence rates of the Patagonian arc against the adjacent South American continental margin. Time-averaged exhumation rates along the Río Rincon anticline (54.6–22 Ma) and along the Río Nutria thrust (46.5–22 Ma) suggest rather low exhumation rates of 1.6–1.2 mm/yr (maximum). The low exhumation rates link back to constantly low subduction rates, resulting in a period of geological quiescence between 46.5 and 22 Ma.

INTRODUCTION

The Patagonian fold-and-thrust belt is located at the southern tip of South America. Its large curved structure shapes the western Patagonian margin, starting from a N-S orientation at around 51°S to a nearly E-W orientation in Tierra del Fuego (Fig. 1). In the studied Ultima Esperanza District, the structurally deformed Cretaceous strata have been affected by N-S–trending thrusts, back thrusts, faults, and folds (e.g., Winslow, 1981; Wilson, 1991). The present-day landscape is shaped by large fold systems like the Silla syncline, and it offers excellent rock exposures with which to study the timing and thermal evolution of fold-and-thrust belt formation.

The orogen, in its present shape, is the result of long-lasting, polyphase deformation processes occurring during the Late Cretaceous to the early Miocene, as well as late Cenozoic glaciation processes (Wilson, 1991; Fosdick et al., 2011; García et al., 2014). The initial stage of the fold-and-thrust belt formation is marked by a compressional phase and the closure of the precursor Rocas Verdes Basin due to the coeval opening of the Atlantic Ocean and subduction along the Pacific margin (e.g., Dalziel et al., 1974; Bruhn et al., 1978). Thrust loading due to crustal shortening caused flexural subsidence and resulted in the formation of a foredeep in the Magallanes Basin and the depositional environment for deep-marine sediments recorded as the Punta Barrosa and Cerro Toro Formations (Natland et al., 1974; Winn and Dott, 1979; Dalziel, 1981; Wilson, 1991; Fildani and Hessler, 2005; Romans et al., 2009). After a roughly 30 m.y. period of active foreland basin sedimentation, the eastward-propagating thrust front progressively incorporated the Upper Cretaceous Punta Barrosa and Cerro Toro Formations into the fold-and-thrust belt (e.g., Wilson, 1991). The position of the present orogenic front is attributed so far to a major Miocene deformational event (Kraemer, 1998; Fosdick et al., 2013).

Various geochronological methods, such as K-Ar dating on magmatic biotite (Altenberger et al., 2003) and U/Pb dating on detrital and ash-bed zircons (e.g., Fildani et al., 2003; Romans et al., 2010; Bernhardt et al., 2012), as well as low-temperature tools such as (U-Th)/He dating

†annette.suessenberger@unige.ch; susanne.schmidt@unige.ch; kwemmer@gwdg.de; lukas.baumgartner@unil.ch; bernard.grobety@unifr.ch.

GSA Bulletin; May/June 2018; v. 130; no. 5/6; p. 975–998; https://doi.org/10.1130/B31766.1; 13 figures; 2 tables; Data Repository item 2017371; published online 5 December 2017.

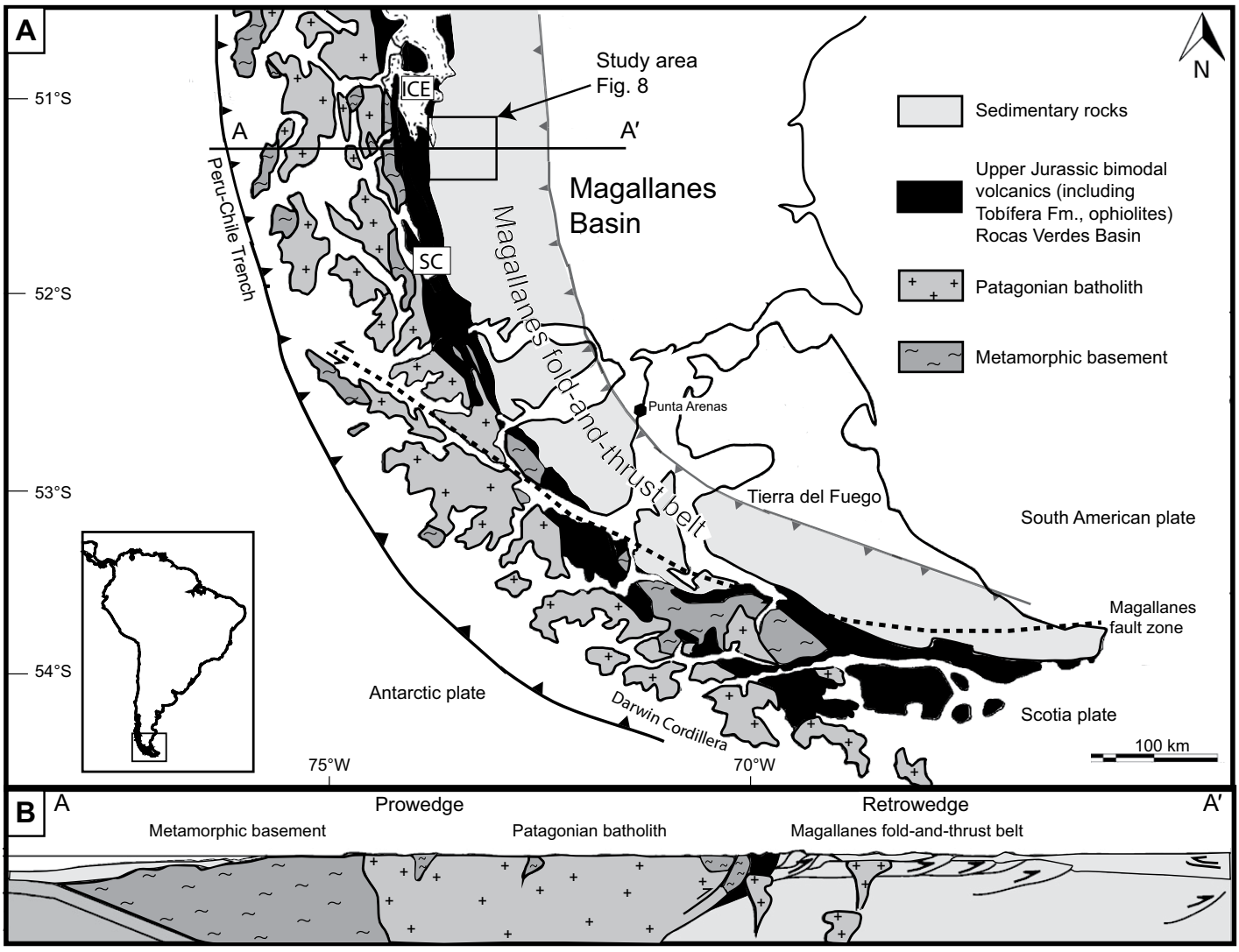

Figure 1. (A) Simplified geological map with the main geological units and the location of the study area (Fig. 8) in the Ultima Esperanza District marked by a black rectangle (50 km × 50 km). The Upper Jurassic bimodal volcanic rocks include the Tobífera Formation and the Sarmiento ophiolite complex, representing remnants of the Rocas Verdes Basin. SC—Sarmiento complex; ICE—South Patagonian ice shield. Map is modified from Dalziel (1981) and Hanson and Wilson (1993). (B) Generalized structural cross section A-A′ showing the present-day tectonic situation of the Patagonian orogenic wedge, modified after Fosdick et al. (2013).

on apatite (Thomson et al., 2010) and zircon (Nelson, 1982; Fosdick et al., 2013), have been used to reconstruct the deformational and thermal history of the Magallanes Basin. U/Pb zircon dating contributed important constraints for the stratigraphic record and fold-and-thrust belt initiation, whereas low-temperature chronology records the last stage of uplift. However, no precise age data for the main phase of thrusting and thrust-driven rock uplift exist in the literature due to the lack of thrust exposure and thrust-related rocks such as fault gouges. Winslow (1982) stated that stratigraphic units in the deepest part of the basin were folded in the Middle Tertiary and observed a diachronicity progressing from the SE to the NW. Fosdick et al. (2011) defined a broad period of thrust activity between 74 and 27 Ma based on crosscutting relationships. Biddle et al. (1986) and Wilson (1991) considered that an incomplete stratigraphic record from 60 to 45 Ma might have been caused by a deformational phase and uplift in the hinterland.

The present study addresses the time interval of major folding and thrusting and provides the missing piece for a better understanding of fold-and-thrust belt formation within the Ultima Esperanza District. We approached this question by the combined use of clay characterization and K-Ar dating of at least two different illite fine fractions, generally <0.2 µm and <2 µm. Detailed illite mineral characterization played a pivotal role in deciphering the relationship between the low-temperature thermal overprint related to regional burial and deformational events in the complex setting of the thrust-folded Magallanes foreland basin. The K-Ar ages of synkinematically grown illites were interpreted in the context of a metamorphic pattern and their relationship to thermal events active at different times in the study area. The illite characterization included the determination of the crystallization parameter, polytype quantification, and scanning and transmission electron (SEM, TEM) and optical microscopic studies. Several different terminologies can be used to characterize the low-temperature-pressure conditions of initial metamorphism. In this paper, we used the Kübler index (KI) to express illite crystallini-

ties (Kübler, 1967) and the metamorphic zones of Winkler (1976); correlation of KI values and metamorphic zones was conducted according to Merriman and Frey (1999) and Abad (2007).

GEOLOGIC SETTING

The study area is located between 51°S and 51°20′S latitude and forms part of the Patagonian fold-and-thrust belt, situated at the western margin of the Magallanes retroarc basin (Fig. 1; e.g., Winslow, 1981; Biddle et al., 1986; Wilson, 1991). The sedimentary, structural, and metamorphic history of the Magallanes Basin is related to the opening and closure of the precursor Rocas Verdes Basin, followed by the formation and uplift of the Andean orogenic belt (e.g., Biddle et al., 1986). The Magallanes Basin was filled throughout the Cretaceous with an ~7-km-thick sedimentary sequence, starting with deep-marine sediments and succeeded by shallow marine up to deltaic sediments (Fig. 2; e.g., Dalziel et al., 1974).

Formation of the Rocas Verdes Basin

The formation of the Rocas Verdes Basin started during the Middle to Late Jurassic and was related to an extensional phase caused by the breakup of southern Gondwana (Bruhn et al., 1978; Gust et al., 1985; Pankhurst et al., 2000). The Rocas Verdes Basin extended N-S over more than 600 km and narrowed generally from south to north as the result of more rapid and prolonged extension to the south (de Wit and Stern, 1981). The extensional phase climaxed in the formation of quasi-oceanic crust exposed as ophiolites (Sarmiento complex) and bimodal volcanism in the backarc basin (e.g., Dalziel, 1981; Pankhurst et al., 2000; Stern and de Wit, 2003; Calderón et al., 2007). The sedimentary fill of the basin is represented by the Tobífera and Zapata Formations. The Tobífera Formation is the earliest basin-filling unit, and it consists of predominantly volcanic rocks and minor mudstones and has an overall thickness of 1000 m (Katz, 1963; Wilson, 1991) in the Ultima Esperanza District. Fossil assemblages constrain its Upper Jurassic time span of deposition from Oxfordian to Tithonian (Natland et al., 1974; Fuenzalida and Covacevich, 1988; Wilson, 1991). The extensional phase persisted throughout the Early Cretaceous. In its late stage, the basin was filled with a uniform sequence of deep-marine, mud-rich sediments of the Zapata Formation, formerly described as Erezcano Formation (Cecioni, 1957). The overall thickness of the Zapata Formation varies between 1000 and 1200 m (Cortés, 1964). Determination of the depositional age is hampered by difficulty in finding the precise stratigraphic limit between the Zapata Formation and overlying Punta Barrosa Formation. Hence, the maximum depositional time span for the Zapata Formation ranges from Jurassic to early Turonian (Fig. 2; Fildani et al., 2003; Fildani and Hessler, 2005). Based on biostratigraphic observations, shorter periods of deposition were proposed by Katz (1963), i.e., late Tithonian to Albian age (Fig. 2), and Cortés (1964), i.e., late Tithonian to late Aptian (Fig. 2).

Basin Transition from Backarc to Foreland and Early Fold-and-Thrust Belt

The inversion of the tectonic regime from extension to compression and the associated closure of the backarc Rocas Verdes Basin at the end of the Early Cretaceous were caused by higher spreading rates in the South Atlantic Ocean and accelerated subduction rates along the Pacific margin (Rabinowitz and LaBreque, 1979; Dalziel, 1986; Ramos, 1989). Thrust loading of heavy oceanic crust due to incipient fold-and-thrust belt formation triggered flexural subsidence, resulting in the development of a foredeep and the birth of the Magallanes foreland basin stage (Natland et al., 1974; Winn and Dott, 1979; Dalziel, 1981; Biddle et al., 1986; Wilson, 1991; Fildani and Hessler, 2005). This dramatic conversion in depositional environment is reflected by a sudden change in sediment supply observed between the Zapata and Punta Barrosa Formations. The transition is marked by a gradual increase in thickness and abundance of individual sand layers intercalated with mudstones (e.g., Wilson, 1991; Fildani et al., 2003). The sandstone layers were probably derived from calc-alkaline magmatic-arc terrains and metamorphic basement complexes in the hinterland and were deposited by marine gravity flows (Dott et al., 1982; Fildani and Hessler, 2005). Therefore, the psammitic layers at the basal Punta Barrosa Formation are considered to reflect the rapid growth of the magmatic arc and subsequent uplift and erosion. They mark the onset of fold-and-thrust belt formation (e.g., Dalziel et al., 1974; Dott et al., 1982; Wilson, 1991).

Upper Cretaceous to Paleogene Depositional Phase in the Magallanes Basin

The foredeep of the Magallanes foreland basin was filled with deep-marine sediments, recorded as the Punta Barrosa and Cerro Toro Formations (Natland et al., 1974; Winn and Dott, 1979; Dalziel, 1981; Wilson, 1991; Fildani and Hessler, 2005; Romans et al., 2009). Due to their syntectonic deposition, both units pinch out toward the east. The Sarmiento ophiolitic complex and the Canal de las Montañas shear zone are considered as important source areas for the deep-water deposits (Wilson, 1991; Romans et al., 2010; Fosdick et al., 2011; Calderón et al., 2012).

The general thickness of the Punta Barrosa Formation is less than 1000 m (Allen, 1982; Wilson, 1991). Skarmeta and Castelli (1997) even revised the thickness downwards to ~500 m. The depositional environment is confined to a 100-km-wide trough oriented parallel to the westward-adjacent orogenic front (Fildani and Hessler, 2005; Bernhardt et al., 2011). U/Pb zircon ages range from ca. 101 Ma from an interbedded tuff (Fosdick et al., 2011; see Fig. 2) to detrital ages of ca. 92 Ma (Fildani et al., 2003; see Fig. 2). Determinations based on fossil assemblages constrain a time span from Albian to Cenomanian age (Cortés, 1964; see Fig. 2) and from late Aptian to Cenomanian age (Skarmeta and Castelli, 1997).

The transition between the Punta Barrosa and Cerro Toro Formations is gradual and marked by the dominance of shale in the latter (Katz, 1963). The overall thickness of the Cenomanian to Campanian Cerro Toro Formation is 2500 m, including multiple conglomeratic layers of about 400 m thick (Katz, 1963; Scott, 1966; Winn and Dott, 1979; Wilson, 1991; Crane and Lowe, 2008). The conglomeratic unit was deposited in a southward-directed axial submarine channel system (e.g., Hubbard et al., 2008). The depositional environment has been interpreted as a wedge-top depozone (Bernhardt et al., 2011; Ghiglione et al., 2014). In the study area, the deposition of the Cerro Toro Formation commenced around 89.5 Ma (U/Pb volcanic ash zircon) and lasted until 81.7 Ma (U/Pb detrital zircon), with a southward trend of rejuvenation (Bernhardt et al., 2012; see also Fig. 2). Slightly younger U/Pb zircon crystallization ages of 86 Ma were found in volcanic ash layers in sedimentary strata of the Sierra del Toro (Bernhardt et al., 2012; see Fig. 2). Depositional time spans based on fossil assemblages are between Cenomanian and Santonian (Cortés, 1964; Natland et al., 1974; see Fig. 2) and between early Santonian and late Campanian (Katz, 1963; see Fig. 2).

The Cerro Toro Formation grades upward into the Campanian Tres Pasos and Maastrichtian Dorotea Formations, recording a change from deep-water to more deltaic deposits (Katz, 1963; Natland et al., 1974; Macellari et al., 1989; Wilson, 1991; Covault et al., 2009; see Fig. 2). The Tres Pasos Formation reflects a southward-prograding submarine slope system and consists dominantly of sandstones (lower part) and mudstones (upper part; Shultz et al., 2005; Covault et al., 2009). The sandstone-dominated shallow-

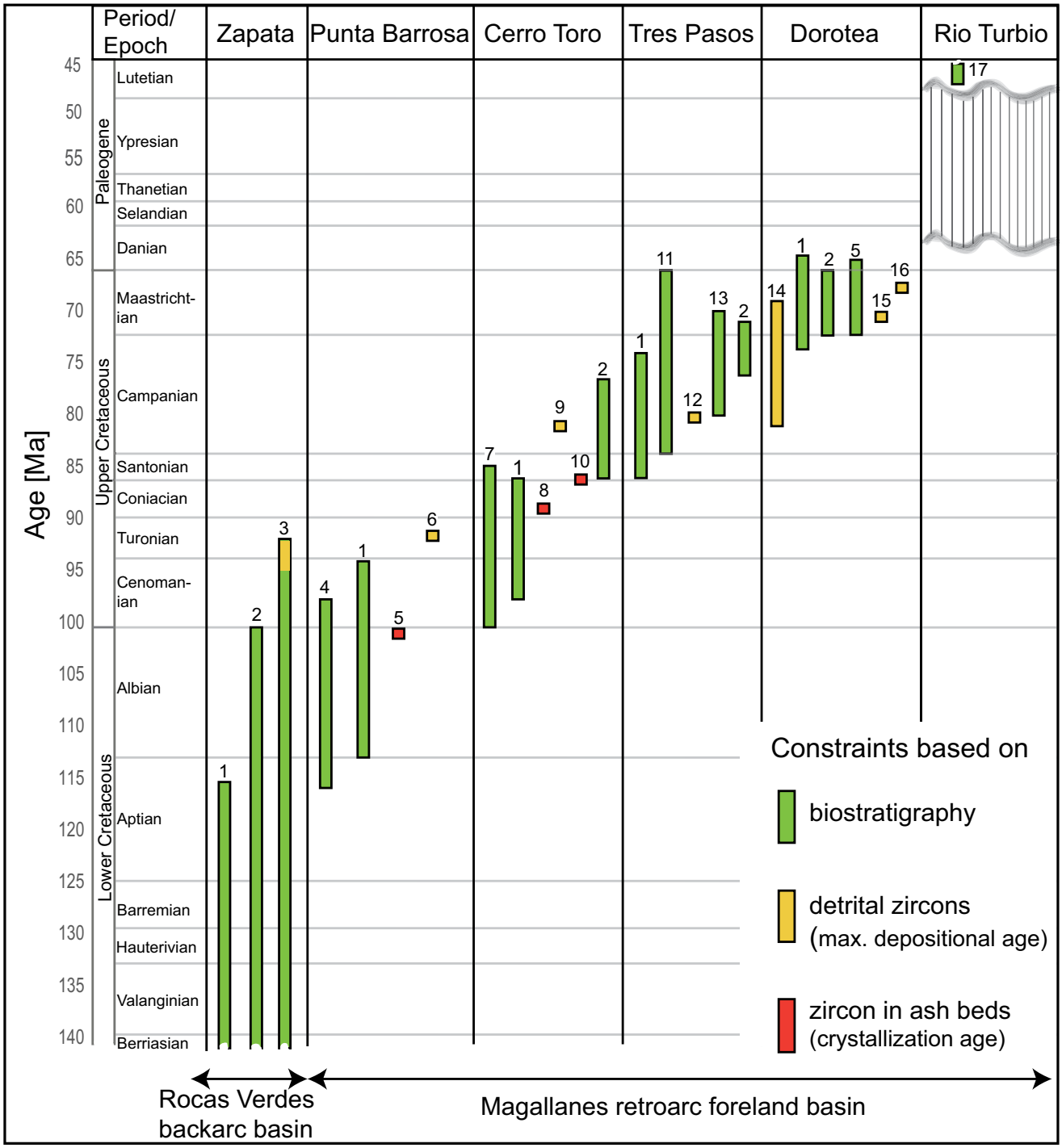

Figure 2. Compilation of existing stratigraphic ages for the Cretaceous stratigraphic units within the Ultima Esperanza District (51°S). Radiometric U/Pb zircon dates were derived from interbedded volcanic ash layers and lava flows (crystallization age) and from detrital zircon populations (maximum depositional age). The U/Pb detrital zircon maximum depositional data are in good agreement with biostratigraphical findings. References: (1) Cortés (1964); (2) Katz (1963); (3) B. Aguirre-Urreta defined the lower limit by an ammonite assemblage (written commun. *in* Fildani and Hessler, 2005); Fildani et al. (2003) defined the upper limit using detrital zircons; (4) Skarmeta and Castelli (1997); (5) Fosdick et al. (2011): 101 ± 1 Ma; (6) Fildani et al. (2003): 92 ± 1 Ma; (7) Natland et al. (1974); (8) Bernhardt et al. (2012): 89.5 ± 1.9 Ma at the Silla syncline; (9) Bernhardt et al. (2012): 81.8 ± 3.7 Ma at the Silla syncline; (10) Bernhardt et al. (2012): 86 ± 1.3 Ma at the Sierra del Toro; (11) Winn and Dott, (1979); (12) Romans et al. (2010): ca. 80 Ma; (13) Natland et al. (1974) and Macellari et al. (1989); (14) Schwartz et al. (2016); (15) Romans et al. (2010): 71.9 ± 2.2 Ma from the lowermost Dorotea Formation; (16) Fosdick et al. (2015): 68.6 ± 1.4 Ma from the uppermost Dorotea Formation; (17) Malumián and Caramés (1997), Malumián (1999): mid-Eocene to Eocene/Oligocene.

water Dorotea Formation records the last filling unit of the Magallanes foredeep, and it was deposited in a progradational axial foreland basin (Katz, 1963; Hubbard et al., 2008; Covault et al., 2009; Romans et al., 2009). Detrital U/Pb zircon ages and biostratigraphical findings indicate a dominantly Campanian depositional age for the Tres Pasos Formation and a largely Maastrichtian depositional age for the Dorotea Formation (Katz, 1963; Cortés, 1964; Natland et al., 1974; Winn and Dott, 1979; Romans et al., 2010; Fosdick et al., 2011, 2015; Bernhardt et al., 2012; Schwartz et al., 2016; see Fig. 2). The Dorotea Formation is separated from the Eocene, shallow-marine Río Turbio Formation by a major regional unconformity (e.g., Biddle et al., 1986; Malumián and Caramés, 1997). The erosional unconformity marks a late episode of fold-and-thrust belt formation (Schwartz et al., 2012). The overall thickness of the sandstone- and siltstone-dominated Río Turbio Formation is around 800 m. Ages based on biostratigraphy suggest a mid-Eocene to Eocene/Oligocene depositional age (Malumián and Caramés, 1997; Malumián, 1999).

Structural Architecture

The Ultima Esperanza District can be divided from west to east into: (1) the basement domain, marked by thick-skinned deformation, and two fold-and-thrust belt domains, comprising (2) the internal domain and (3) the less-deformed external domain (after Kraemer, 2003; Ghiglione et al., 2009). The study area is entirely situated in the internal domain, and it is limited by the east-dipping, basement-seated Zapata thrust to the west and the Toro thrust to the east. Within the internal domain, the main frontal structures are indicated by N-S–trending, west-dipping thrusts, back thrusts, and series of anticlines and synclines (e.g., Winslow, 1981; Wilson, 1983, 1991; Altenberger et al., 2003). The Río Rincon anticline marks the early Paleogene frontal thrust into the foreland basin (Fosdick et al., 2011).

In the westernmost part of the study area, the Tobífera and Zapata Formations are broadly folded and thrusted and have undergone low-grade metamorphism (Wilson, 1991; Hervé et al., 2007). East-directed large-scale thrusting gradually progressed toward the foreland. West of the Torres del Paine intrusive complex, a shallowly west-dipping detachment of the Zapata thrust between the Zapata and Tobífera Formations exhibits top-to-the-east shear sense and reverse drag (Wilson, 1983; Fosdick et al., 2011). Generally, the Tobífera thrust is postulated to be a foreland-dipping duplex (Wilson, 1983).

Lower and initial Upper Cretaceous units in the western part of the study area, i.e., Zapata and Punta Barrosa Formations, are tightly folded, thrust-faulted, and mostly upright plunging to the east (Fig. 3C; e.g., Wilson, 1991). In the eastward-adjacent foreland-vergent imbricate thrust zone, younger stratigraphic units (i.e., Cerro Toro Formation) are less deformed and are characterized by broad kilometer-scale folds plunging <10° to NNW (e.g., Altenberger et al., 2003). An abrupt change in the wavelength and amplitude of the Silla syncline can be observed between the folded sedimentary strata separated by the Lago Nordenskjöld fault zone (Figs. 3A and 3B; Altenberger et al., 2003). The Punta Barrosa Formation is displaced atop of the Cerro Toro Formation by the Río Nutria thrust sheet, which was first mapped by Cortés (1964). Wilson (1983) and Skarmeta and Castelli (1997) described its prolongation south of the Torres del Paine intrusive complex. Ghiglione et al. (2009) introduced an E-W–striking transfer fault transecting the Torres del Paine intrusive complex to accommodate along-strike variations.

SAMPLING STRATEGY, MATERIAL, AND ANALYTICAL METHODS

The field work and sampling strategy were broadly conceived to cover a regionally meaningful set of samples. Locations close to assumed thrust zones were additionally sampled because they are prone to give information about thrust-related exhumation and associated cooling. Sampling was confined to dark-gray–black pelitic shales, also referred to as mudstone in the study area (Fig. 4). This lithology is superior to other lithologies such as sandstone in recording recrystallization and deformation during fold-and-thrust belt formation. In slates and shales, clay minerals are oriented parallel to S_0 and have undergone compaction. During tectonic horizontal shortening, clay minerals crystallized along the developing cleavage S_1, and the shale fractured along S_0 and S_1 into pencil-shaped units. This pencil cleavage (Figs. 4A, 4B, and 4C) is an important field indicator for incipient metamorphism and deformation.

In total, 23 metapelitic samples belonging to the stratigraphic units of the Tobífera, Zapata, Punta Barrosa, and Cerro Toro Formations were prepared for microscopic, diffraction, and isotopic analyses (Tables 1 and 2). Sample locations with respect to stratigraphic formations and tectonic setting are reported in Table 1. All analytical details can be found in the Data Repository.[1]

[1]GSA Data Repository item 2017371, XRD and K-Ar analytical procedures, is available at http://www.geosociety.org/datarepository/2017 or by request to editing@geosociety.org.

The metapelitic samples were crushed, sieved, and separated by centrifugation according to their grain size following the procedure described by Moore and Reynolds (1997). The different grain-size fractions (<0.2, <2, and 2–6 µm) were subjected to X-ray diffraction (XRD), K-Ar dating, and transmission electron microscopy (TEM). The XRD measurements were performed at the University of Geneva. The diffractograms were used for qualitative phase determination (HighScore Plus), determination of the illite crystallinity and illite peak decomposition (Newmod© on [001] peak), and the quantification of illite polytypes. The TEM analysis was performed on single illite grains in the laboratory of the Swiss Accident Insurance Fund (SUVA, Lucerne, Switzerland). The K-Ar dating on different illite fine fractions was carried out at the University of Göttingen using a Thermo Scientific ARGUS VI mass spectrometer. The K-content was determined by flame photometry. Optical microscopy and secondary scanning electron microscopy (SEM) were performed at the University of Geneva on polished thin sections in order to study the textural relationship of different illite generations.

X-Ray Diffraction Study

The illite crystallinity, or KI value, was used to determine the metamorphic grade by measuring the full width at half maximum (FWHM) of the illite (001) peak at 10 Å in $\Delta°2\Theta$ (Kübler, 1964, 1967). The illite crystallinity is a function of the crystallite thickness, the amount of crystal defects, and the peak interference with illite-smectite interlayering (Merriman et al., 1990; Ferreiro Mählmann et al., 2012). Limits between fields of diagenesis, the anchizone and epizone, are given by 0.42 $\Delta°2\Theta$ and 0.25 $\Delta°2\Theta$, respectively (Kübler, 1967). The anchizone is subdivided into the low (0.42–0.30 $\Delta°2\Theta$) and high anchizone (0.30–0.25 $\Delta°2\Theta$). The limit between high and low epizone is defined by 0.2 $\Delta°2\Theta$. The anchizone is generally assigned to a temperature range between 200 °C and 300 °C (e.g., Merriman and Frey, 1999).

Illite Peak Decomposition

The 10 Å illite peak can be decomposed into a well-crystallized illite (WCI), a poorly crystallized illite (PCI), and, under diagenetic conditions, also into an illite-smectite component (I/S). The PCI component usually contains <5% smectite, whereas the WCI is almost pure illite. The I/S component is an illite-rich mixed-layer phase with usually >95% illite.

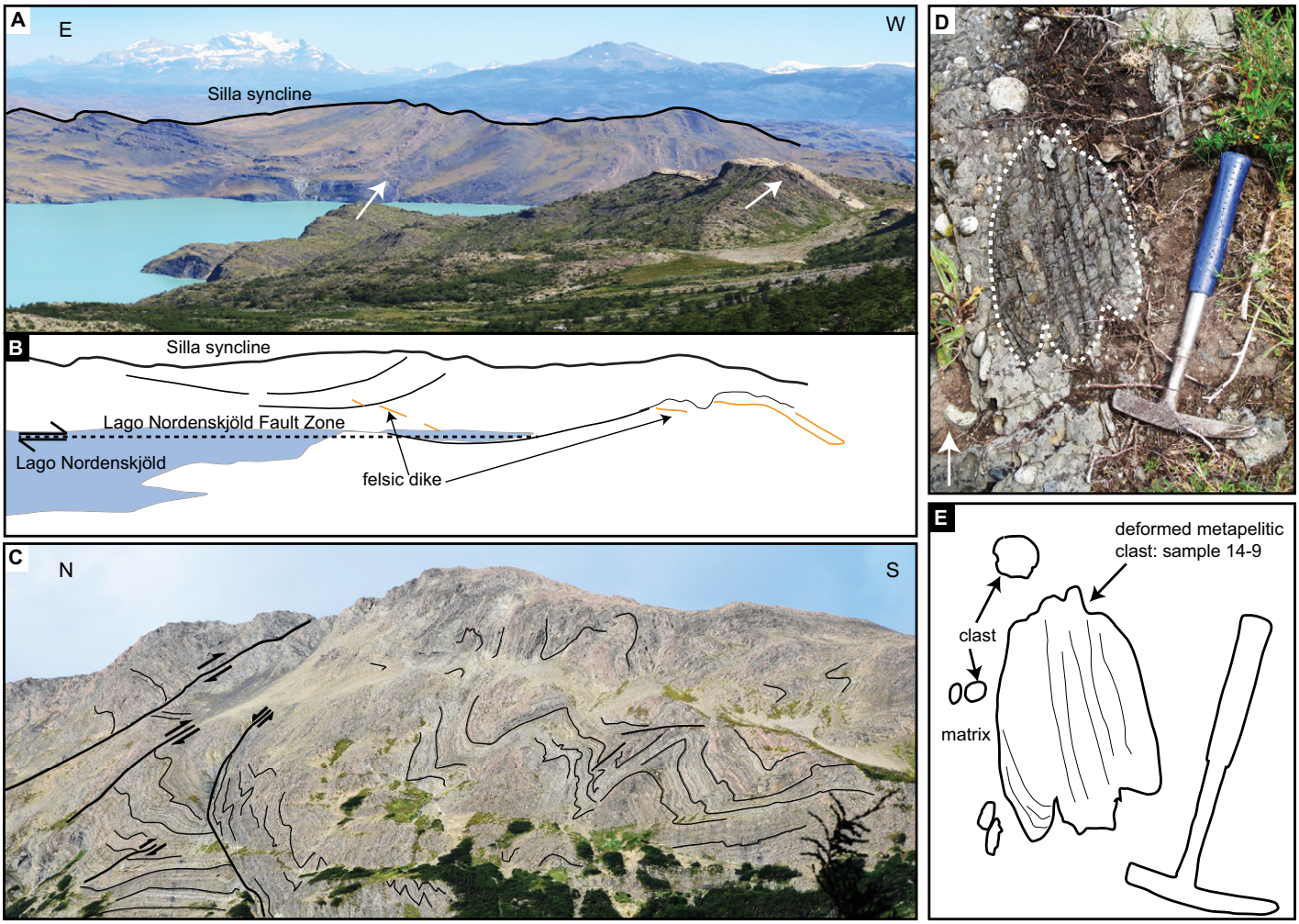

Figure 3. (A) Kilometer-scale open Silla syncline in the Cerro Toro Formation at Lago Nordenskjöld. View is from the base of Mount Almirante Nieto looking south. White arrows point to the dike indicated in B. (B) Schematic sketch of the Silla syncline as in A. The fold axis is truncated by a felsic dike. The Lago Nordenskjöld fault zone accommodates along-strike variation in the Silla syncline. The distance between the shore lines is 1.3 km. (C) Thrust-folded Punta Barrosa Formation at the Sierra Chacabuco/Cordillera Arturo Prat. Different styles of folding are observed: conjugate kink-bands, kink-like folds, and chevron folds. Outcrop length = ~1 km. (D) Deformed metapelitic clast in the Cerro Toro conglomerate at the western limb of the Silla syncline. Sample 14-9. Hammer length = 28 cm. White arrow points stratigraphically upward. (E) Schematic sketch of D.

Illite Polytype Quantification

Generally, three illite polytypes can be distinguished: $1M_d$, 1M, and $2M_1$ (e.g., Środoń and Eberl, 1984). With increasing temperature, illite polytypes undergo a transformation from $1M_d$ via 1M to ultimately $2M_1$ illite (e.g., (Hunziker et al., 1986). Temperature estimations for $1M_d$/1M formation are thought to be <200–210 °C, whereas $2M_1$ is formed at temperatures >280 °C (Yoder and Eugster, 1955; Velde, 1965; Weaver, 1989). The transformation of $2M_1$ to $1M/1M_d$ illite during retrograde metamorphism (i.e., cooling) occurs less frequently (e.g., Zhao et al., 1999; Abad et al., 2003).

Fundamental Concept of K-Ar Dating and Detrital Age Calculation

Illite, as a K-bearing clay mineral, is widely used for K-Ar and $^{40}Ar/^{39}Ar$ geochronology and has proven to be an important tool in deciphering diagenetic and low-grade metamorphic events (e.g., Clauer and Chaudhuri, 1995; Dong et al., 1997; Dong et al., 2000). K-Ar ages and their equivalent $^{40}Ar/^{39}Ar$ total-gas-fusion ages (encapsulated) assume that there is no K at sites that are not Ar-retentive (i.e., crystal surfaces or crystal defects). Because this assumption is not always valid, K-Ar ages have to be regarded as minimum ages. According to Dong et al. (1995, 1997) and Fitz-Díaz et al. (2016), $^{40}Ar/^{39}Ar$ retention ages account for K that may not contribute to the accumulation of ^{40}Ar (i.e., K present in exposed half layers, smectite layers, and dislocations) and should be considered as maximum ages. The K-Ar dating technique relies on closed-system behavior, assuming that neither loss nor gain of ^{40}Ar or ^{40}K has occurred since illite formation. The K-Ar closing temperature for illite fine fractions (<0.2 µm, <2 µm) is poorly constrained to date. Early studies reported a closure temperature interval (end of significant diffusion of ^{40}Ar) for mica fractions (<2 µm) in the order of 260 ± 30 °C (Hunziker et al., 1986). Other authors found indications that fine-grained white micas (sericite <2 µm) did not behave as an open system, even at tem-

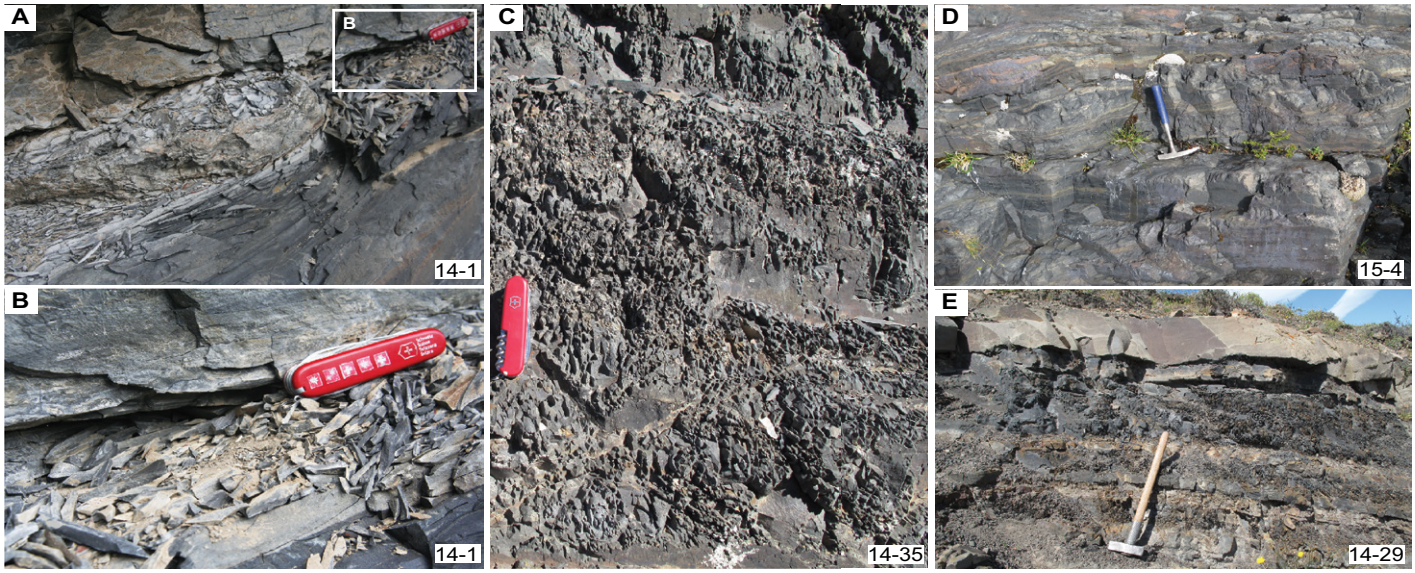

Figure 4. Examples of typical rock lithologies. (A) Pencil-shaped sample 14-1 from the Punta Barrosa Formation. Pocketknife for scale = 8.5 cm. (B) Close-up of sample 14-1 as indicated in A; pocketknife for scale = 8.5 cm. (C) Pencil-shaped black metapelite of the Cerro Toro Formation. Mirador Lago Sarmiento. Sample 14-35. Pocketknife for scale = 8.5 cm. (D) Outcrop of sample 15-4 located east of Laguna de los Tres, Zapata Formation. Hammer length = 28 cm. (E) Road cut close to sample location 14-29 at the entrance "Guarderia Laguna Amarga," Cerro Toro Formation. Hammer length = 60 cm.

peratures of 275 °C (Wemmer and Ahrendt, 1997). The upper limit of the closure temperature for mica was constrained to around 350 °C (Purdy and Jäger, 1976).

Diagenetic to anchizonal shales often contain a complex mixture of authigenic and detrital illites. In shales of this very low-grade environment, authigenic illites are reflected by the $1M/1M_d$ illite polytype, and detrital illite is reflected by the $2M_1$ illite polytype. As a consequence of the illite polytype mixture, the age spectra are usually inclined, with the youngest age in the finest grain-size fraction and the oldest age in the coarsest grain-size fraction (Pevear, 1992, 1999). The obtained K-Ar ages reflect the different proportions of different illite populations and should be interpreted as a mixed age (e.g., Pevear, 1992; Środoń et al., 2002). Mixed ages might also result from long-lasting illitization processes related to the burial history (Środoń et al., 2002). The K-Ar ages tend to decrease with decreasing grain size. This observation has often been attributed to the decreasing detrital contamination of smaller grain sizes rather than to $^{40}Ar^*$ loss (e.g., Perry, 1974; Pevear, 1992). In fact, even the smallest grain size will always contain some contamination of older polytypes, and the ages have to be regarded as maximum ages at first sight. Pevear (1992) demonstrated that calculation of the "true" diagenetic age and "true" detrital age is possible by using the linear relationship between the % detrital illite ($2M_1$) and K-Ar ages. By plotting the K-Ar ages of at least three size fractions of illite against the percentage of detrital illite ($2M_1$), extrapolation to 0% detrital illite gives the age of diagenesis, and extrapolation to 100% $2M_1$ illite gives the age of detrital illite formation.

RESULTS

Analytical results are summarized in Table 2.

Modal Rock Composition

Most samples show a very homogeneous mineral composition, with illite as the most prominent clay mineral (Table 2). Albite, chlorite, and quartz are frequent mineral phases. Plagioclase appears most frequently as albite. Patches of An-rich plagioclase within albite are relicts of incomplete albitization. Chlorite occurs as clinochlore or chamosite and oc-

TABLE 1. COMPILATION OF ANALYZED SAMPLES WITH THEIR RESPECTIVE LOCALITIES, LITHOLOGY, AND STRATIGRAPHIC INFORMATION

Sample ID	UTM 18S		Lithology	Stratigraphic formation	Tectonic setting
14-1	0648871	4318572	Metapelite	Punta Barrosa	Thrust zone with maximum rock uplift
14-6	0642825	4332968	Metapelite	Cerro Toro	Foreland-vergent imbricate thrust zone
14-7	0643918	4333779	Metapelite	Cerro Toro	Foreland-vergent imbricate thrust zone
14-9	0643448	4333592	Metapelite	Cerro Toro	Foreland-vergent imbricate thrust zone
14-11	0629175	4334443	Metapelite	Cerro Toro	Thrust zone with maximum rock uplift
14-15	0656071	4344726	Metapelite	Cerro Toro	Foreland-vergent imbricate thrust zone
14-21	0659707	4361604	Metapelite	Cerro Toro	Foreland-vergent imbricate thrust zone
14-29	0654794	4350359	Metapelite	Cerro Toro	Foreland-vergent imbricate thrust zone
14-35	0649435	4344518	Metapelite	Cerro Toro	Foreland-vergent imbricate thrust zone
14-38	0641688	4322630	Metapelite	Cerro Toro	Foreland-vergent imbricate thrust zone
14-43	0700747	4333238	Metapelite	Cerro Toro	Thrust zone with maximum rock uplift
14-46	0666468	4287315	Metapelite	Cerro Toro	Foreland-vergent imbricate thrust zone
14-55	0660345	4341604	Metapelite	Cerro Toro	Foreland-vergent imbricate thrust zone
14-63	0647592	4353236	Metapelite	Cerro Toro	Foreland-vergent imbricate thrust zone
14-71	0633043	4340985	Metapelite	Punta Barrosa	Thrust zone with maximum rock uplift
14-72	0633306	4340357	Metapelite	Punta Barrosa	Thrust zone with maximum rock uplift
14-75	0641118	4339153	Metapelite	Cerro Toro	Foreland-vergent imbricate thrust zone
15-4	0620955	4336994	Metapelite	Zapata	Thrust zone with maximum rock uplift
15-21	0641861	4322337	Metapelite	Punta Barrosa	Thrust zone with maximum rock uplift
15-29	0647346	4311214	Metapelite	Tobífera	Thrust zone with maximum rock uplift
16-4	0662106	4364353	Metapelite	Cerro Toro	Foreland-vergent imbricate thrust zone
16-12	0647651	4350213	Metapelite	Cerro Toro	Foreland-vergent imbricate thrust zone
16-22	0633950	4302218	Metapelite	Punta Barrosa	Thrust zone with maximum rock uplift

Note: Universal Transverse Mercator (UTM) Zone 18S.

TABLE 2. MINERALOGY, POLYTYPES, ILLITE CRYSTALLINITIES, AND K/Ar AGE DATA FOR DIFFERENT GRAIN-SIZE FRACTIONS

Sample ID	Size (µm)	Mineralogy							Illite polytype (%)		10 Å illite peak decomposition			Illite crystallinity		K_2O (wt%)	$^{40}Ar^*$ (nL/g, @STP)	$^{40}Ar^*$ (%)	Age (Ma)	±2σ (Ma)	Interpretation	Event
		Qz	Ill	I/S	Chl	C/S	Plg	Others	$1M_d$/1M	$2M_1$	WCI	PCI	I/S	KICis	KIKü							
14-1	<0.2	+++	+++	+	+	–	++	kln(o), ttn(o)	37	63	35	53	12	0.30	0.26	5.52	10.46	90.66	57.8	0.7	Cooling age	3
	<2	+++	+++	+	++	–	++	kln(o), ttn(o)	25	75	59	17	24	0.29	0.25	4.99	10.36	90.60	63.2	1.2	Cooling age	3
14-6	<2	+++	++	+	++	–	++	bt(o)	69	31	25	63	12	0.41	0.36	2.85	8.14	92.01	86.4	0.9	Mixed age	1
14-7	<0.2	++	+++	+	++	+	+		85	15	24	69	7	0.38	0.32	5.28	12.77	91.10	73.4	1.8	Mixed age	1
	<2	++	++	+	++		++	ttn(o)	57	43	17	71	12	0.40	0.34	4.28	12.72	91.68	89.9	1.8	Mixed age	1
	2–6	+++	++	–	++	–	++		25	75	25	67	8	0.31	0.27	2.69	10.70	90.44	119.5	2.3	Mixed age	
14-9	<2	+++	++	–	++		++	ttn(o)	19	81	60	31	9	0.29	0.24	4.13	13.46	92.32	98.3	1.2	Cooling age	1
14-11	<0.2	+++	+	+	++	+	+		85	15	32	50	18	0.41	0.35	5.06	9.14	81.58	55.1	0.7	Maximum age	4
	<2	+++	++	+	++	o	++		80	20	52	35	13	0.33	0.29	3.63	7.90	79.94	66.2	1.4	Mixed age	
14-15	<0.2	+++	++	+	++		+	kln(o)	81	19	20	58	22	0.35	0.3	4.8	9.73	90.34	61.9	0.7	Maximum age	3
	<2	+++	+	+	++		+	kln(o)	nd	nd	36	44	20	0.38	0.33	3.6	9.49	90.08	79.9	1.8	Mixed age	2
14-21	<0.2	+++	++	++	++	+	+	ant(o)	82	18	14	50	36	0.57	0.49	5.11	11.17	86.92	66.5	0.8	Maximum age	3
	<2	+++	++	+	++	+	++		62	39	21	52	27	0.45	0.41	4.2	11.13	87.81	80.3	2.8	Mixed age	2
14-29	<0.2	+++	++	++	+++	++	o	kln(o)	70	30	15	59	26	0.59	0.5	5.7	10.89	90.75	58.3	0.6	Maximum age	3
	<2	+++	+++	+	+++	–	+	kln(o)	59	41	39	34	27	0.35	0.31	4.48	11.37	91.35	77	1.2	Mixed age	2
14-35	<0.2	+++	++	+	++		++		81	19	40	35	25	0.5	0.43	4.69	9.58	91.23	62.2	3.5	Maximum age	3
	<2	+++	++	+	++	o	++		63	37	50	31	19	0.37	0.32	3.63	9.58	89.97	80	1.3	Mixed age	2
14-38	<0.2	+++	+	+	++	o	++	kln(o)	74	26	19	61	20	0.33	0.28	4.98	10.97	92.32	67.1	0.8	Maximum age	3
	<2	+++	++	+	++	–	++		nd	nd	29	54	19	0.41	0.35	3.81	10.57	89.82	84	1.1	Mixed age	2
14-43	<0.2	+++	++	+	++	+	+	bt(o), kln(o)	86	14	33	56	11	0.35	0.31	5.73	8.63	90.03	46.2	0.6	Maximum age	4
	<2	+++	++	+	++	o	++	bt(o)	84	16	32	65	3	0.38	0.33	4.19	7.59	90.45	55.3	1.1	Cooling age	4
	2–6	+++	++	–	++	–	++	bt(o)	63	37	nd	nd	nd	0.27	0.23	2.37	5.70	91.64	73.1	1.1	Mixed age	
14-46	<0.2	+++	++	+	++	o	+	bt(o)	73	27	22	25	53	0.55	0.47	5.39	10.97	90.89	62.1	0.7	Maximum age	3
	<2	+++	++	+	++	o	++		67	34	33	32	35	0.48	0.41	4.04	10.77	92.05	80.8	1	Mixed age	2
	2–6	+++	++	o	++	–	+++		60	40	nd	nd	nd	0.3	0.26	2.24	9.43	91.43	126.3	2	Mixed age	
14-55	<0.2	+++	++	+	++		+	ant(o)	72	28	14	59	27	0.8	0.67	5.8	10.35	79.60	54.5	1.1	Maximum age	3
	<2	+++	++	+	++	–	+	bt(o)	63	37	36	57	7	0.36	0.31	3.9	10.47	85.64	81.5	1.1	Mixed age	2
14-63	<0.2	+++	++	++	++	+	++	bt(o)	86	14	29	44	27	0.42	0.37	4.72	9.71	91.81	62.7	1	Maximum age	3
	<2	+++	++	+	++	+	++	bt(o)	nd	nd	39	46	15	0.38	0.33	4.07	10.76	92.14	80.1	1.1	Mixed age	2
	2–6	+++	++	+	++	–	++	bt(o)	nd	nd	51	49	0	0.3	0.26	2.38	8.91	93.28	112.4	1.7	Mixed age	
14-71	<2	++	+++	o	++	–	++		73	27	55	32	13	0.32	0.28	4.02	7.01	77.99	53.3	1.1	Maximum age	4
14-72	<0.2	++	++	+	++	o	++		90	10		nd	nd	0.41	0.35	6.25	9.74	92.82	47.6	1.5	Cooling age	4
	<2	++	+++	+	++	–	++		73	27	36	56	8	0.41	0.36	5.29	10.56	93.36	60.8	1.1	Cooling age	3
	2–6	+++	++	+	++	–	++	py(o)	46	55	nd	nd	nd	0.29	0.24	3.09	8.77	93.94	85.9	1.3	Mixed age	
14-75	<0.2	++	++	++	++	+	+	kln(o)	92	8	30	56	14	0.4	0.34	5.57	10.56	91.14	57.8	0.6	Cooling age	3
	<2	+++	++	+	++	+	++	ttn(o)	63	38	33	50	17	0.42	0.36	4.18	10.59	90.01	76.9	1.3	Mixed age	2
	2–6	+++	+	–	++		+++	ttn(o), py(o)	23	78	nd	nd	nd	0.25	0.22	2.45	9.45	90.65	115.8	1.8	Mixed age	
15-4	<0.2	++	+++		o		o		24	76	49	43	8	0.29	0.24	8.15	12.56	79.09	47.2	0.6	Cooling age	4
	<2	+++	+++	–	o	–	o	glt(o)	18	82	87	13	0	0.2	0.17	8.02	14.06	81.18	53.6	0.9	Cooling age	4
15-21	<2	+++	++	–	++	–	+		26	74	58	42	0	0.25	0.22	5.82	8.86	87.86	46.5	5.2	Cooling age	4
15-29	<2	+++	+	–	+++	–	++	bt(o)	21	79	68	32	0	0.26	0.23	2.36	4.22	39.20	54.6	1.4	Cooling age	4
16-4	<2	+++	++	+	+++	+	++	py(o)	69	31	12	54	35	0.57	0.48							
16-12	<2	++	+++	+	++	+	+	kln(o)	72	28	35	53	13	0.35	0.31							
16-22	<2	+++	++	–	+++	–	++	ttn(o)	9	91	74	26	0	0.25	0.22							

Note: Mineral abbreviations: Qz—quartz; Ill—illite; I/S—illite-smectite interlayering; Chl—chlorite; C/S—chlorite-smectite interlayering; Plg—plagioclase; kln—kaolinite; ttn—titanite; bt—biotite; py—pyrite; ant—anatase; glt—glauconite; +++—major component; ++—significant component; +—minor component; o—present in traces; "–"—not identified. Phase identification is based on X-ray diffraction. $1M_d$ (d—disordered), 1M and $2M_1$ are illite polytypes with different degrees of disorder in their stacking sequence. WCI—well-crystallized illite; PCI—poorly crystallized illite; I/S—illite-smectite interlayering; KICis—Kübler index calibrated on Cis limits; KIKü—Kübler index calibrated on Kübler limits. $^{40}Ar^*$—radiogenic argon; STP—standard pressure and temperature conditions; nd—not determined. (1) Early Cenomanian (98 Ma)—Illite formation during beginning of fold-and-thrust belt formation. (2) Early Campanian (ca. 80 Ma)—Illite growth during diagenesis and burial metamorphism. (3) Early Paleocene (ca. 60 Ma)—Illite formation during thrusting. (4) Early Eocene (ca. 55–46 Ma)—Illites affected by uplift processes.

casionally as pennantite. Biotite is generally of detrital origin. A few diagenetic to anchizonal samples show illite-smectite and chlorite-smectite interlayering. More psammitic samples, which experienced higher anchimetamorphic conditions, display newly grown epidote. Apatite, zircon, Ti-oxide phases, calcite, halloysite, and pyrite occur frequently as accessory minerals. Rare allanite, monazite, and sphalerite are present, sometimes newly formed along (001) planes during the chloritization of detrital biotite. Fine dispersed organic matter is present in various proportions. A general trend of decreasing quartz and increasing clay mineral content is observed from coarse- to fine-grained size fractions.

Optical Microscopy, SEM, and TEM

Secondary electron and optical microscopy revealed textures typical for diagenetic/low-anchizonal to epizonal conditions (Figs. 5 and 6). Diagenetic to anchizonal samples exhibit up to four distinct illite occurrences: (1) illite occurring in grain interstices and/or in porous interspaces assigned to diagenesis (Fig. 6A); (2) arbitrarily oriented illite in the matrix or in miarolitic cavities corresponding to syn- or postdiagenetic growth (Figs. 5A, 6A, and 6B); (3) oriented illite growing on foliation planes, suggesting a synkinematic origin (Fig. 6C); and (4) recrystallized illite along rims of detrital mica occurring during prograde and retrograde metamorphism (Figs. 5B and 6E). Detrital micas are recognized based on their elongated crystal shape, which differ conspicuously in appearance from the micaceous matrix minerals (Figs. 5B, 6A, and 6D). The detrital micas often feature diagenetic bending and recrystallized rims of either illite or chlorite, which may exhibit interstratification (Figs. 5B and 6E). Well-crystallized illites ($2M_1$) are characterized by their platy habit as observed in SEM (Fig. 7B). Occasionally, authigenic zoned illite indicates a polyphase growth (Fig. 5C). Detrital biotite is frequently altered into chlorite and is associated with newly formed allanite, monazite, titanite, and sphalerite along its (001) planes (Fig. 6A). Spheroidal clusters of polyframboidal pyrite

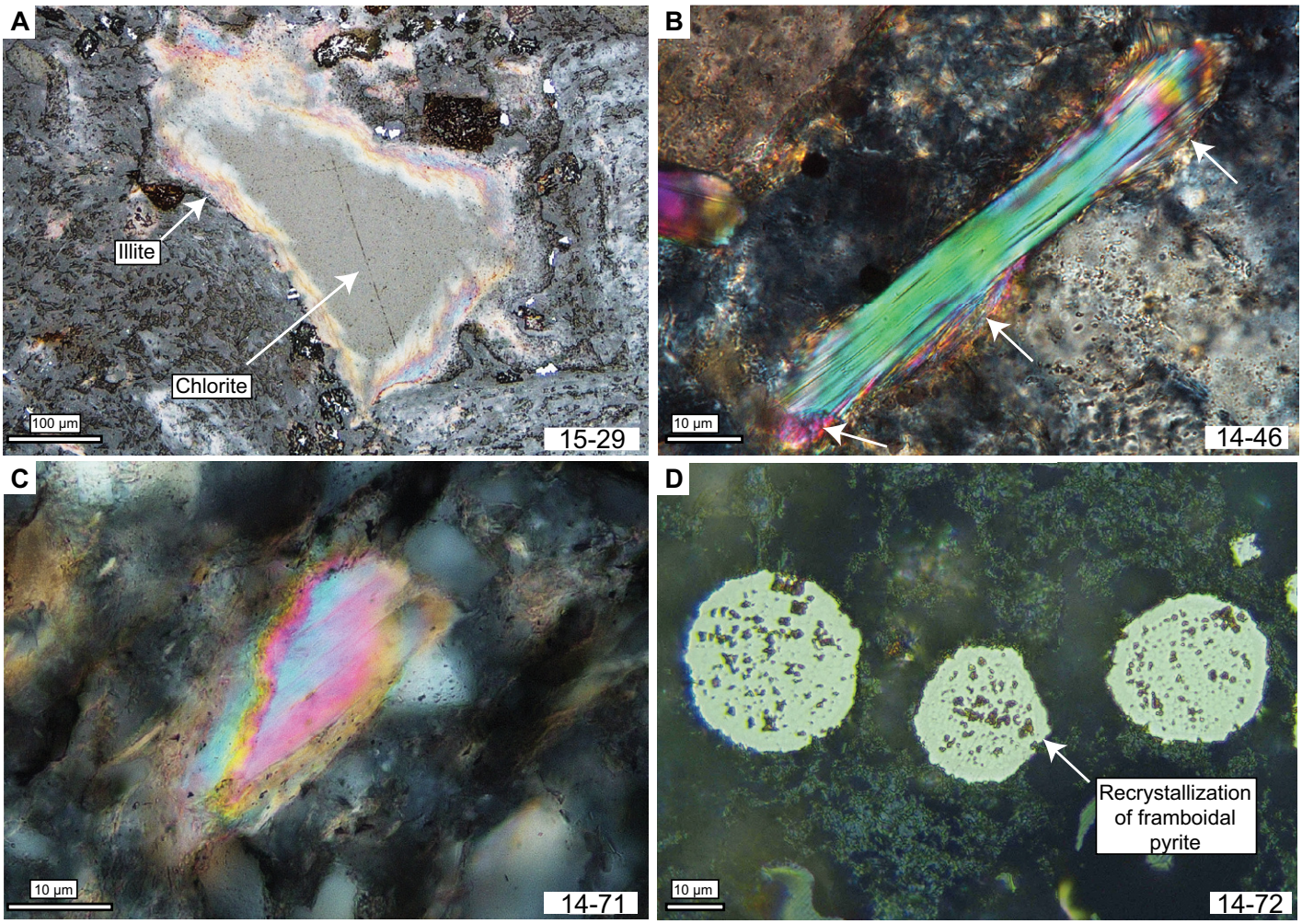

Figure 5. Photomicrographs showing representative illites from different metamorphic conditions. (A) Clay minerals filling a miarolitic cavity. The filling often starts with well-crystallized illite, indicated by higher interference colors at the rims, and continues with well-crystallized chlorite; combination of reflected light, crossed nicols (+N), and oil immersion; sample 15-29. (B) Detrital muscovite with recrystallized rims (indicated by white arrows) in a diagenetic sample; +N; sample 14-46. (C) Zonation of authigenic illite; +N and oil immersion; sample 14-71. (D) Recrystallization of framboidal pyrite developing first crystallographic planes visible at grain edges (white arrow); reflected light; sample 14-72.

composed of micron-sized euhedral crystals are frequently present in late diagenetic to low-anchizonal samples (Fig. 6F). High-anchizonal to epizonal samples show recrystallization to a more homogeneous pyrite crystal (Fig. 5D).

Based on the K-Ar results and their regional position within the thrust zone of maximum rock uplift, two samples were selected for TEM study: 14-1 (<2 µm) and 15-21 (<0.2 µm). The TEM images reveal new growth of 1M illite (Figs. 7A, 7C, and 7D) and the presence of $2M_1$ illite (Fig. 7C). With respect to the epizonal temperatures in both samples, the 1M illite is interpreted as a retrograde phase. The lattice fringe image of sample 14-1 depicts a 7 Å spacing, typical for kaolinite, at the mineral rim of a 1M illite. The kaolinite replacing illite is interpreted as a late-stage low-temperature alteration event.

KI and 10 Å Peak Decomposition

The KI for 23 metapelites was determined in the <0.2 µm and <2 µm clay fractions. The data range from 0.24 to 0.67 Δ°2Θ in the <0.2 µm and 0.17–0.48 Δ°2Θ in the <2 µm fraction (Table 2). The values indicate diagenetic to high anchimetamorphic conditions with occasional lower epizonal values (Fig. 8). A decreasing trend of metamorphic conditions is observed toward the foreland basin located in the east. Diagenetic values are observed in the eastern part of the study area (Laguna Azul) at the stratigraphically uppermost part of the Cerro Toro Formation. Samples of the Cerro Toro Formation generally depict anchimetamorphic conditions regardless of their stratigraphic position. For instance, samples located on a 20-km-long, E-W–trending corridor confined by the Lago Nordenskjöld and Lago Sarmiento (samples 14-75, 14-35, 14-38, 14-15) show constant low-anchizonal conditions with KI values between 0.30 and 0.36 Δ°2Θ in the <2 µm fraction (Fig. 8). Samples located in the western part of the study area show dominantly high-anchizonal to low-epizonal KI values. The highest metamorphic degrees are observed in samples of the Zapata Formation located in the west of the study area: east of the Laguna de los Tres (sample 15-4) and in the Punta Barrosa and Tobífera Formations close to the fold axis of the Río Rincon anticline (samples 14-1, 15-21, 15-29, and 16-22; Fig. 8).

Illite peak decomposition reveals WCI and PCI as principal components. The proportion of WCI/PCI correlates well with the KI values (Fig. 9). The amount of WCI is highest in epizonal

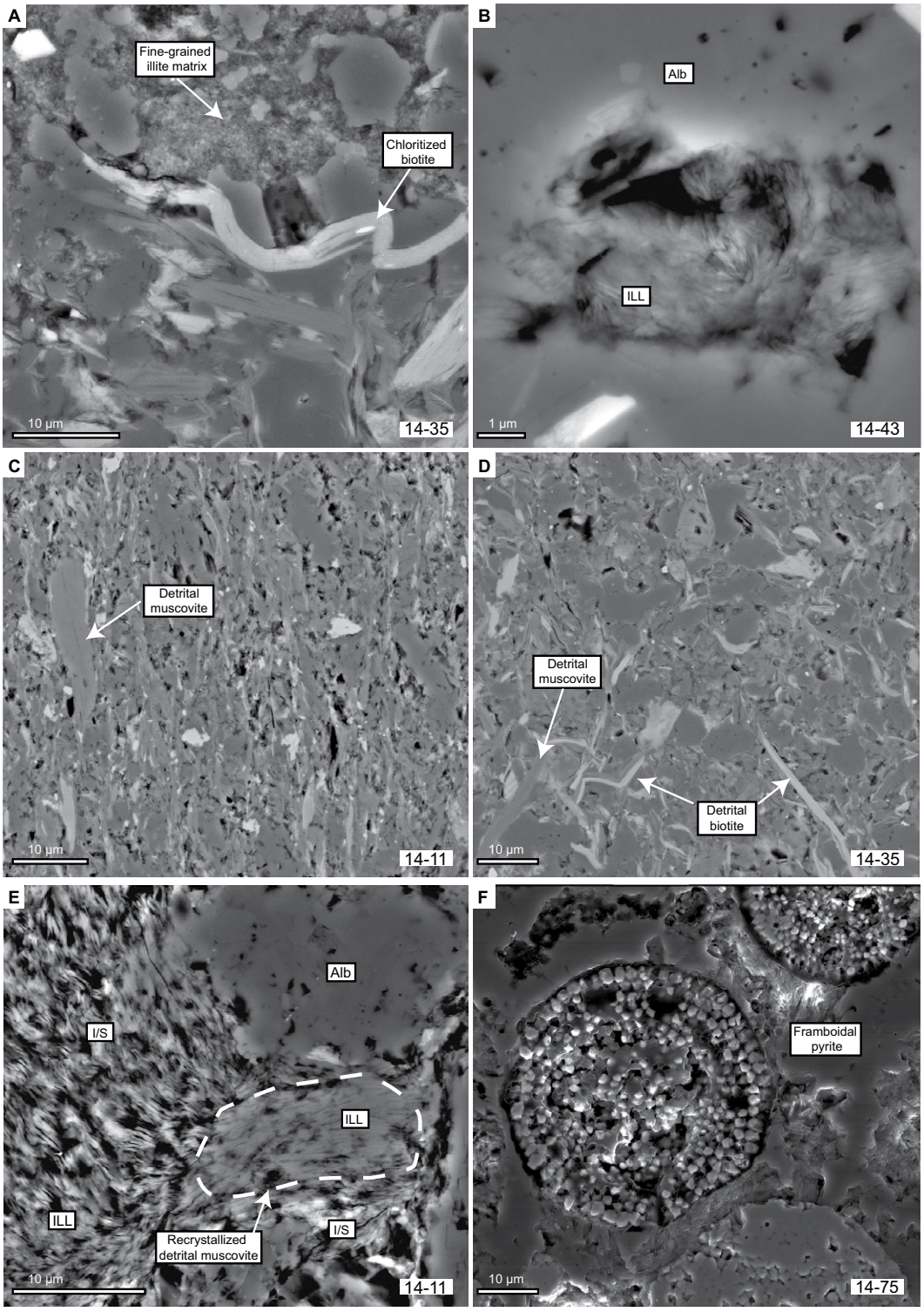

Figure 6. Backscattered and secondary electron microscope (BEM, SEM) images: (A) Fine-grained authigenic illite in the matrix and detrital micas. Sample 14-35. (B) Arbitrarily oriented illite growing in a cavity of albite. Sample 14-43. (C) Beginning alignment (N-S) of phyllosilicates along the cleavage plane in a matrix of coarser-grained detrital grains. Sample 14-11. (D) Texture of an anchizonal metamorphic sample. No preferred orientation of authigenic illite is observed. Detrital muscovite and biotite are indicated by the white arrows. Sample 14-35. (E) Recrystallization of a detrital muscovite outlined by the white dashed line. The newly crystallized illite and illite/smectite are merging into the matrix. Sample 14-11. (F) SEM image of framboidal pyrite in a low-anchizonal sample. Sample 14-75. Alb—albite, ILL—illite, I/S—illite/smectite.

rocks and decreases under anchizonal conditions. The WCI component ranges from 12% to 87%, and the PCI component varies between 13% and 71% (Table 2). Generally, I/S interlayering occurs in amounts of less than 25%. In anchizonal samples, WCI and PCI show about equal distribution, occasionally slightly shifted in favor of PCI.

K-Ar Ages

K-Ar ages were obtained for the <0.2 µm and <2 µm clay fractions as well as for six samples from the 2–6 µm fraction of 20 metapelitic samples (see Data Repository for analytical details [footnote 1]). The K_2O content ranges from 2.24 to 8.15 wt%, and the radiogenic Ar (*Ar) content samples from 39.2% to 93.9%, indicating reliable analytical conditions (Table 2). A general trend of decreasing age with decreasing grain size is observed (Fig. 10). The K-Ar ages vary between 73.4 ± 1.8 Ma and 46.2 ± 0.6 Ma in the <0.2 µm size fraction, between 98.3

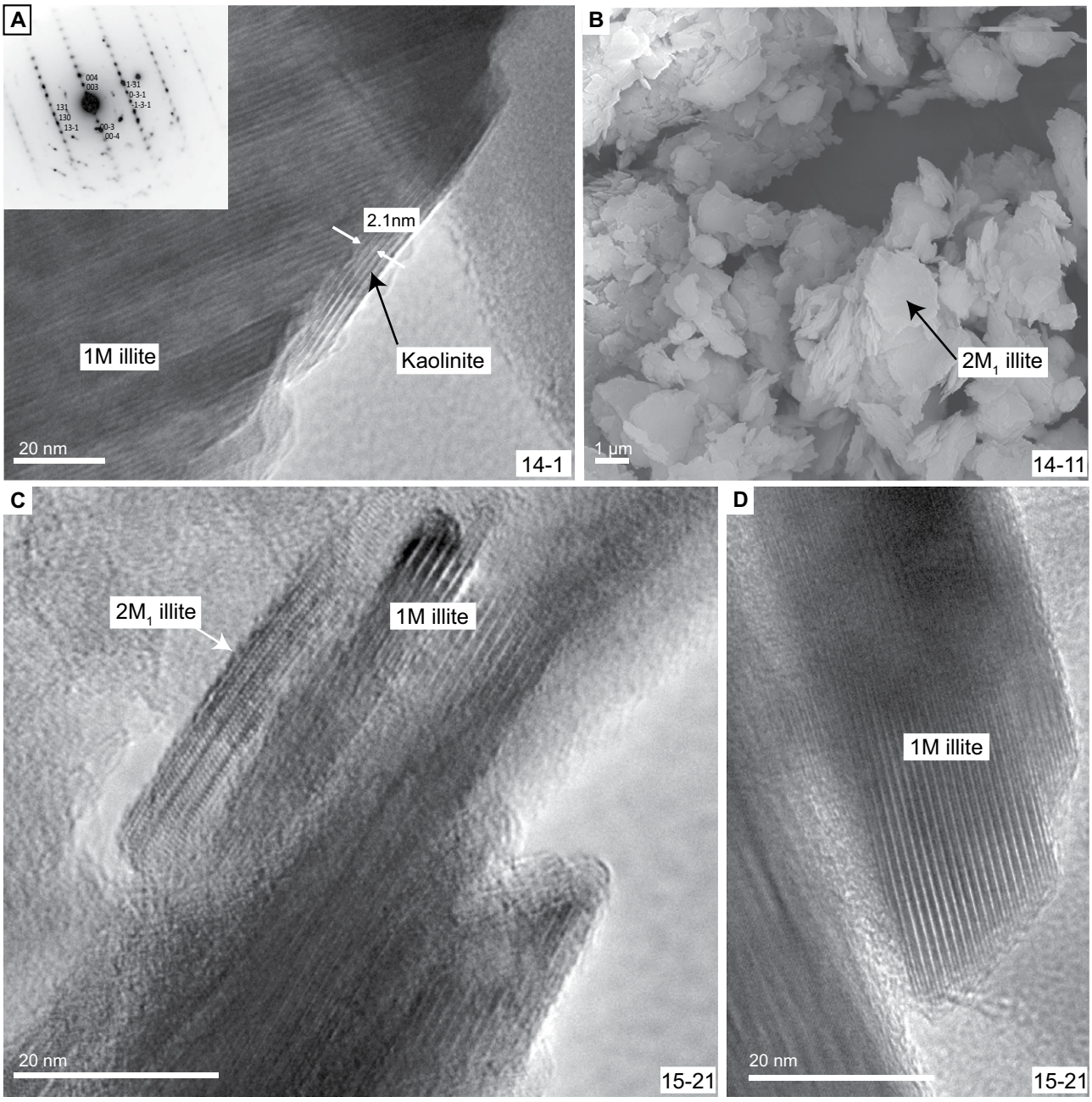

Figure 7. Transmission and secondary electron microscope (TEM, SEM) images of different illite polytypes: (A) Lattice fringe image of 1M illite (10 Å spacing). The lattice fringes bracketed by the white arrows have a 7 Å spacing characteristic for kaolinite. Selected area diffraction pattern in the upper-left corner reveals a dominant $1M_d$ illite with minor $2M_1$ ordering. Inverted image contrast. Sample 14-1, <2 µm fraction. (B) SEM image of platy $2M_1$ illite. Sample 14-11. (C) TEM image with lattice fringes of ordered $2M_1$ and disordered 1M illite. Sample 15-21, <0.2 µm fraction. (D) Lattice fringe image of 1M illite. The lattice fringes are long and straight. Sample 15-21, <0.2 µm fraction.

± 1.2 Ma and 46.5 ± 5.2 Ma in the <2 µm size fraction, and between 126.3 ± 2.0 Ma and 73.1 ± 1.1 Ma in the 2–6 µm illite fraction (Table 2; Figs. 11A and 11B). The age spread within different size fractions of a single sample can be considerably variable, ranging from 5 to 60 m.y. (Table 2; Fig. 11B). The probability age distributions shown in Figure 10 reveal five discrete age populations that vary with grain size. In the first group, samples of the Cerro Toro Formation (n = 4) yielded K-Ar ages between ca. 130 Ma and 115 Ma in their 2–6 µm fraction. A second peak (n = 1) was recorded by sample 14-9, yielding a K-Ar age in the <2 µm fraction of 98.3 ± 1.2 Ma; it is thus older than comparable metapelitic samples from the same succession (samples 14-7 and 14-6). This sample is a metapelitic clast in the Cerro Toro conglomerate in the Silla syncline (Figs. 3D and 3E). A third group (n = 11) yielded ages around 80 Ma in the <2 µm fraction. These samples were located in

the foreland-vergent imbricate thrust zone and belong to the Cerro Toro Formation (samples 14-15, 14-21, 14-29, 14-35, 14-38, 14-46, 14-55, 14-63, and 14-75; Fig. 11A). A fourth group of samples (n = 11) yielded ages of ca. 60 Ma in either both grain-size fractions or solely in the smallest <0.2 µm fraction. They included samples 14-1 and 14-43 of the Punta Barrosa Formation, located in the vicinity of thrust zones, as well as the <0.2 µm fraction of samples located in the foreland-vergent imbricate thrust zone (Fig. 11A). The last group of samples (n = 7) displayed ages around 45 Ma to ca. 55 Ma in either both or one grain-size fraction (<0.2 µm, <2 µm; Figs. 11A and 11B). The youngest samples were found in the western part of the study area, east of Laguna de los Tres (15–4), 200 m below the summit of Cerro Ferrier (14-11), in the hinge zone (15-29) and along the western limb (15-21) of the Río Rincon anticline, and in the vicinity of the Río Nutria thrust south of the Torres del Paine intrusion (samples 14-43, 14-71, and 14-72).

The K-Ar ages of three illite size fractions of samples 14-7 and 14-75 were plotted against the percentage of detrital $2M_1$ illite in order to estimate their "true" detrital and "true" authigenic age (Fig. 12). Both samples originated from the Cerro Toro Formation located in the Silla syncline (Figs. 8 and 11). According to Crane and Lowe (2008), they are part of the Pehoe B member and probably have a stratigraphic age between 89.5 ± 1.9 Ma and 81.8 ± 3.7 Ma (Bernhardt et al., 2012; see Fig. 2). Extrapolating the $2M_1$ content to 100% yields a maximum detrital age of 134–138 Ma, whereas extrapolating to 0% $2M_1$ covers a time span for the authigenic illite between 60 and 50 Ma for the Silla syncline.

SYNTHESIS OF OBSERVATIONS AND INTERPRETATION OF K-Ar AGES

Four distinct periods of illite growth were identified based on their K-Ar ages and degree of regional metamorphism: (1) early Cenomanian illite crystallization (98 Ma), (2) widespread early Campanian diagenetic illite growth during long-lasting illitization processes (ca. 80 Ma), (3) significant period of illite formation in the early Paleocene (ca. 60 Ma), and a (4) late stage of illite growth in the early Eocene (55–46 Ma). These thermal events, responsible for illite crystallization, will be discussed within the framework of basin evolution and thrust propagation toward the foreland.

Based on the K-Ar fine fraction ages and KI values, we propose to subdivide the internal domain into a western thrust zone with maximum rock uplift and an eastern foreland-vergent imbricate thrust zone (Figs. 8 and 11).

Figure 8 (*on following page*). (A) Geologic map of the study area in the Ultima Esperanza District with the Kübler index (KI) results of the glycolated <2 µm fraction showing a decreasing metamorphic degree from west to east. Based on K-Ar fine fraction ages and KI values, the internal domain is subdivided into a western thrust zone with maximum rock uplift and an eastern foreland-vergent imbricate thrust zone. Limits between fields of diagenesis, anchizone and epizone, are given by 0.42 Δ°2Θ and 0.25 Δ°2Θ, respectively (Kübler, 1967). The anchizone is subdivided into low (0.42–0.30 Δ°2Θ) and high anchizone (0.30–0.25 Δ°2Θ). The limit between high and low epizone is defined by 0.2 Δ°2Θ. Sample 14-46 is located off the map to the south at the shoreline of Lago Sofia. Map is modified from Fosdick et al. (2011). (B) Schematic cross section as indicated in A, showing the metamorphic pattern in relation to thrust location and stratigraphic position. Note that KI values next to the thrust change due to different stratigraphic levels placed next to each other. All units are given in Δ°2Θ. Structural section is modified from Ghiglione et al. (2009) and Fosdick et al. (2011). (C) Schematic cross section as indicated in A, showing the metamorphic pattern in relation to the Río Rincon anticline. All units are given in Δ°2Θ. Structural section is modified from Fosdick et al. (2011).

(1) Early Cenomanian (98 Ma)—Illite Formation during Initial Fold-and-Thrust Belt Formation

Indications for the onset of deformation were found in a deformed metapelitic clast (sample 14-9) within the Cerro Toro conglomerate (Pehoe B member) in the Silla syncline (Figs. 3D, 3E, 10, 11A, and 12, column A). The conglomerate was deposited in a channel system immediately east of the active thrust front of the Patagonian orogenic belt (Crane and Lowe, 2008).

The mineral composition consists of illite, plagioclase (mainly Ab with minor An relicts), quartz, chlorite, and minor titanite. A dominance of illite/muscovite and chlorite can be observed in the <2 µm fraction (Table 2). The deformed metapelitic clast yielded an age of 98.3 ± 1.2 Ma in the <2 µm fraction (Table 2). The KI value of 0.24 Δ°2Θ in the same grain-size fraction places the sample in the lower epizone, suggesting temperatures close to 300 °C. The relatively high temperature is in good agreement with the observed absence of clay mineral interstratification in the <2 µm fraction. Consequently, the age should be interpreted as the cooling age, and any mixing between a detrital and an authigenic component can be excluded. Remarkably, this sample differs substantially in age and KI value from samples (14-7 and 14-6) taken in stratigraphically deeper metapelitic units of the Silla syncline (lithologic unit IIImd according to Crane and Lowe, 2008). For comparison, these samples yielded anchizonal KI values in the <2 µm fraction (0.34 and 0.36 Δ°2Θ) and slightly younger mixing ages of 89.9 ± 1.8 Ma and 86.4 ± 0.9 Ma, respectively. In this context, the epizonal conditions preserved in the deformed metapelitic clast (sample 14-9) are considered as inherited from the source area. Remarkably, but not unexpectedly, this sample preserved its epizonal metamorphic conditions within the surrounding regional anchizonal rocks. The absence of any response to the surrounding low-grade metamorphic conditions is most likely explained by the protected location (i.e., stress shadow) of the clast. Comparable observations of source area–derived K-Ar ages in phyllitic clasts from an anchizonal conglomerate in the northern Rhenish Massif (Belgium/Germany) were reported by Ahrendt et al. (2001).

The Cenomanian age (98.3 ± 1.2 Ma) of the deformed metapelite (sample 14-9) is significantly older than the stratigraphic age of the conglomerate. According to Bernhardt et al. (2012), the deposition of the Cerro Toro Formation within the Silla syncline is slightly younger than the Sr isotopic age of 87.5 ± 03 Ma and the U/Pb volcanic ash zircon age of 89.5 ± 1.9 Ma (Fig. 2). A U/Pb age of 81.8 ± 3.7 Ma on detrital zircons constrains the upper limit of the stratigraphic age (Bernhardt et al., 2012; Fig. 2). Hence, the clast is unlikely to have a Cerro Toro Formation origin, but belongs instead to an older reworked stratigraphic unit (i.e., Punta Barrosa or Zapata Formation). In this geological context, the age of 98.3 ± 1.2 Ma records a thermal event or an episode of thrusting and unroofing in the hinterland.

(2) Early Campanian (ca. 80 Ma)—Illite Growth during Diagenesis and Burial Metamorphism

Authigenic illite formed during long-lasting burial illitization processes is present in the Cerro Toro Formation located in the foreland-vergent imbricate thrust zone (samples 14-15, 14-21, 14-29, 14-35, 14-38, 14-46, 14-55, 14-63, and 14-75; Figs. 10, 11A, and 11B). The K-Ar results of the <2 µm fraction are discussed next; the results obtained for the corresponding

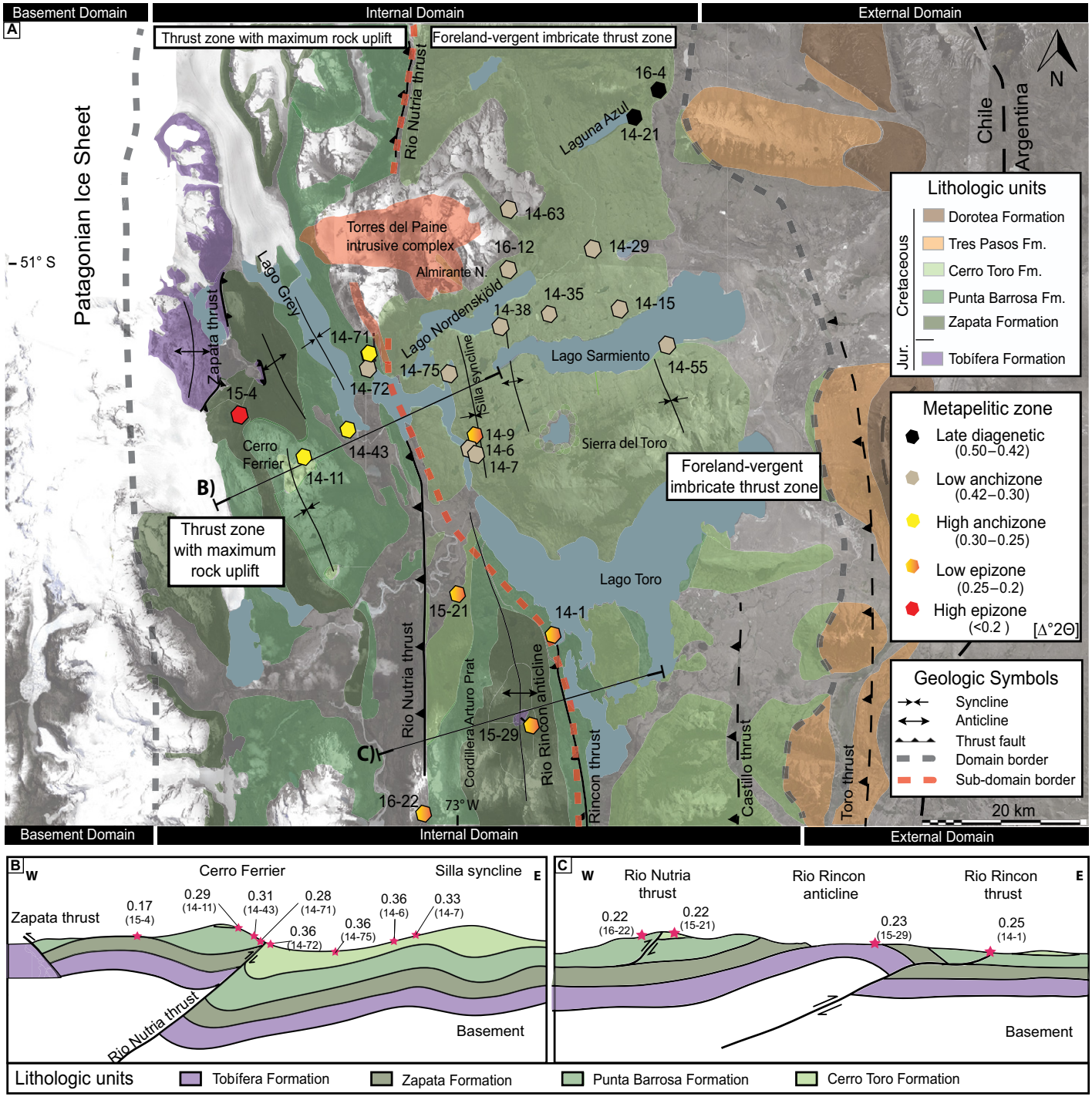

Figure 8.

<0.2 µm fraction are discussed in the section "Early Paleocene (ca. 60 Ma)."

The low-grade, metapelitic mineral assemblage is dominated by illite/muscovite, albite, quartz, detrital biotite, and chlorite (mainly of chamositic composition). Carbonate clasts, framboidal pyrite, titanite, apatite, monazite, sphalerite, and zircon are additional minor components. Backscattered electron (BSE) images reveal textures typical for diagenetic to low-anchizonal conditions (Figs. 6A and 6D). Neither preferred orientations of illite growth nor other textural or mineralogical indications point to elevated temperatures (>250 °C). Optical microscopy as well as BSE images show the occurrence of newly grown illite at the rims of large idiomorphic detrital mica grains (Fig. 5B), in the matrix (Fig. 6A), and in porous interspaces (Fig. 6B). The detrital $2M_1$ mica, occurring in big flakes, shows bending caused by diagenetic compaction (Figs. 6A and 6D). Framboidal pyrite occurs frequently and is of early diagenetic origin (Fig. 6F). Its preservation suggests the absence of later pyrite recrystallization as

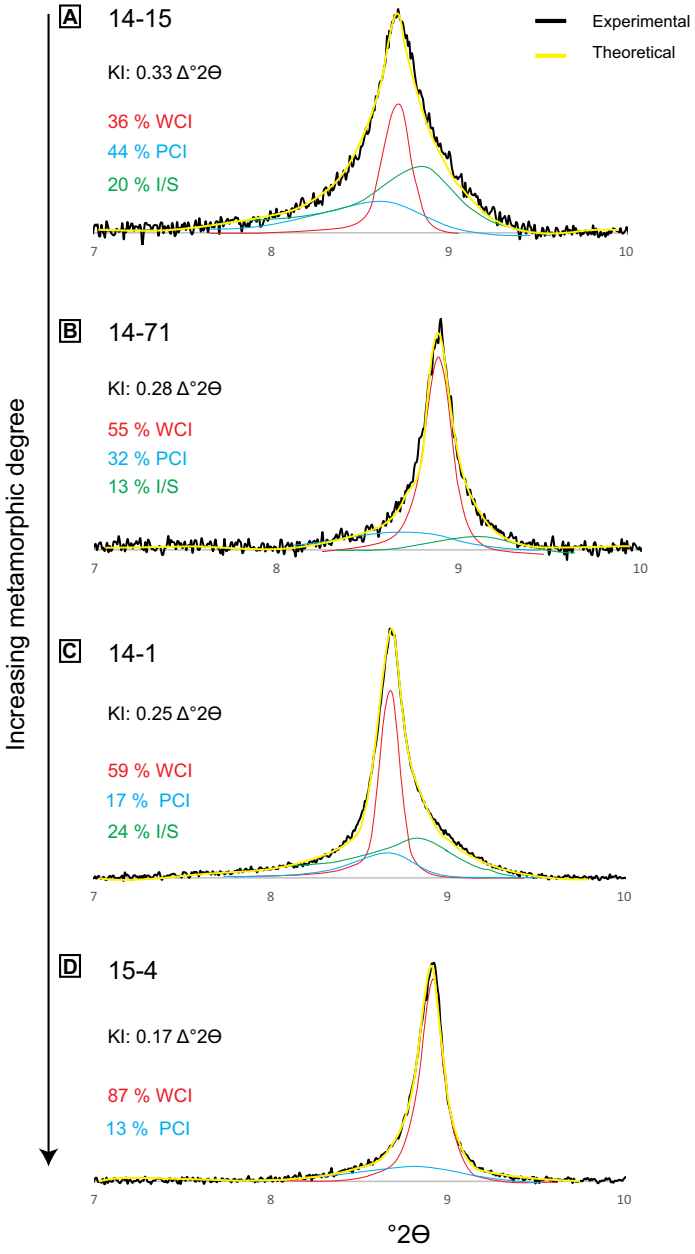

Figure 9. Results of illite peak decomposition after glycolization for four samples (<2 µm) with different illite crystallinities. With increasing metamorphic grade, the amount of well-crystallized illite (WCI) increases. KI—Kübler index; PCI—poorly crystallized illite; I/S—illite-smectite interlayering (illite >90%).

observed in epizonal samples (Fig. 5D) and thus is in agreement with the assumed low temperatures. The formation of framboidal pyrite is generally interpreted to be indicative of low-temperature settings of ~<200 °C (Rickard, 1970; Wilkin and Barnes, 1997). KI values of the <2 µm fraction range between 0.31 and 0.41 Δ°2Θ and indicate mostly low-anchizonal conditions with maximum temperatures around 200–250 °C (Table 2; Fig. 8). These temperatures are in good agreement with zircon (U-Th)/He data, which indicate burial temperatures >190 °C for the uppermost Cerro Toro Formation (Fosdick et al., 2013).

K-Ar analyses on this set of samples yielded ages of ca. 80 Ma in the <2 µm fraction and ca. 60 Ma in the <0.2 µm fraction (Table 2; Figs. 11A and 11B). Since the K-Ar ages of the <0.2 µm fraction give significantly younger ages, the <2 µm ages must be interpreted as mixing ages resulting from low-temperature authigenic and high-temperature detrital illitic components (Figs. 10 and 11B). This interpretation is confirmed by anchizonal metamorphic conditions derived from KI values of the <2 µm fraction, indicating that the temperature was not high enough to reset the detrital age memory of $2M_1$ illite (i.e., temperature <280 °C), but it was sufficient to trigger new growth of 1M illite during burial anchizonal conditions. Additional evidence comes from the asymmetric (001) illite reflection observed by XRD analysis, emphasizing the existence of several illite phases. Peak decomposition reveals a complex assembly of well- and poorly crystallized illite (WCI, PCI) components and I/S interlayering (Fig. 9A). Illite phase quantification indicates a dominant PCI component (i.e., corresponds to authigenic illite) ranging between 31% and 57%, as well as minor WCI and I/S authigenic phases (Table 2).

The interpretation of the <2 µm fraction as a mixing age renders these samples geologically problematic, and only by using the illite polytype quantification method (e.g., Pevear, 1992; Grathoff and Moore, 1996) can a geologically meaningful statement be derived. The two illite polytype end members and their corresponding K-Ar ages were used (i.e., authigenic 1M and detrital $2M_1$) to recalculate the "true" detrital and "true" authigenic ages of two samples (14-7 and 14-75, <0.2, <2, and 2–6 µm fractions) originating from the western limb of the Silla syncline (Fig. 12). An important assumption is that all $2M_1$ illite is detrital in origin, and no $2M_1$ formed through the transformation of 1M illite during diagenetic to anchizonal conditions. Extrapolating the $2M_1$ content to 100% (i.e., 0% $1M/1M_d$) yields a detrital age of 134–138 Ma, and extrapolation to 0% $2M_1$ (i.e., 100% $1M/1M_d$) covers a time span for the authigenic illite between 60 and 50 Ma for the Silla syncline (Fig. 12). The extrapolated detrital illite/muscovite of Valanginian age most likely reflects either reworked Lower Cretaceous sediments or a magmatic source rock of this age. The extrapolated authigenic ages of 60–50 Ma confirm the ages obtained for the same sample set in the <0.2 µm fraction as well as for samples in the western part of the internal domain (i.e., thrust zone with maximum rock uplift), as evident in Figures 10 and 11. These ages document a late phase of illite growth, most probably related to a thermal event induced by thrust burial during wedge thickening. Placing these events in the context of basin evolution provides excellent agreement between stratigraphic and tectonic findings from the literature and this study (Wilson, 1991; Malumián, 1999; Fosdick et al., 2011; Bernhardt et al., 2012; Figs. 11 and 13).

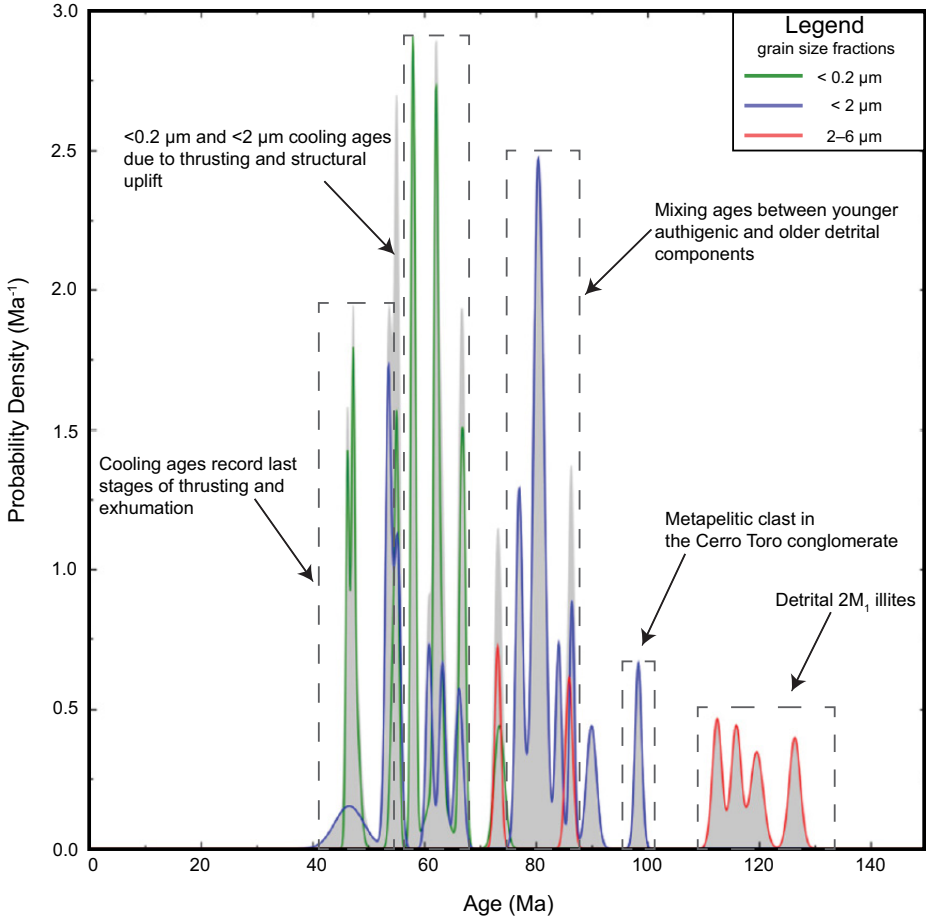

Figure 10. The probability density (Ma^{-1}) vs. age (Ma) plot shows a general trend of decreasing age with decreasing grain size. Five age groups can be distinguished as indicated by the boxes with dashed lines.

(3) Early Paleocene (ca. 60 Ma)—Illite Formation during Thrusting and Structural Uplift

Early Paleocene ages of illite recrystallization were observed for samples from the Cerro Toro and Punta Barrosa Formations (Figs. 11A and 11B, Table 2). Samples 14-1 and 14-72 from the Punta Barrosa Formation were located close to thrust zones and yielded ages of 63.2 ± 1.2 to 60.8 ± 1.1 Ma, indicating an isotopic reset of the <2 µm fraction (Figs. 11A and 11B). Other samples (14-15, 14-21, 14-29, 14-35, 14-38, 14-46, 14-55, 14-63, and 14-75) in the Cerro Toro Formation exhibited early Paleocene dates of illite crystallization only in their <0.2 µm fraction. Their corresponding <2 µm fraction yielded mixing ages, as the temperature was not sufficiently high enough to reset the isotopic system (see previous discussion).

Particular significance is assigned to sample 14-1 (Figs. 4A and 4B), collected in the vicinity of the Río Rincon thrust front. The age for the <0.2 µm fraction is 57.8 ± 0.7 Ma, and the age for the <2 µm fraction 63.2 ± 1.2 Ma. KI values range from 0.26 Δ°2Θ in the fine fraction to 0.25 Δ°2Θ in the coarse fraction, indicating low-epizonal metamorphic conditions with temperatures probably close to 300 °C. As such, the isotopic reset of detrital and diagenetic illite in the coarse fraction is not surprising, and the ages are interpreted as cooling ages. Figure 9C shows the 10 Å basal illite reflection, which can be decomposed into a dominant WCI phase (59%) and a minor PCI phase. Polytype quantification indicates new growth and recrystallization of $2M_1$ illite in both size fractions, reaching up to 75% in the <2 µm fraction and 63% in the <0.2 µm fraction (Table 2). It is important to note that the thoroughly prograde transformation of 1M to $2M_1$ illite in both grain-size fractions during epizonal conditions makes a decisive difference. Therefore, the presence of 1M illite as observed by polytype quantification and peak decomposition (PCI and I/S phase) indicates retrograde crystallization, i.e., at temperatures below peak metamorphic conditions.

TEM images reveal needle-shaped $1M_d$/1M illite accompanied by minor amounts of $2M_1$ illite. The 1M polytype is identified by diffuse streaking (Fig. 7A). The $1M_d$/1M illite is considered as retrograde in origin, as expected from polytype quantification and KI values. Kaolinite occurs at the mineral rim and is identified by its 7 Å lattice fringe periodicity (Fig. 7A). Since the peak metamorphic conditions certainly exceeded the thermal stability field of kaolinite (e.g., Hurst, 1985), the latter is interpreted as a retrograde low-temperature alteration phase replacing illite. Fluid-driven retrograde processes under diagenetic conditions were first described by Nieto and Peacor (1993) as "retrograde diagenesis." They observed retrograde diagenesis on a regional scale caused by fluid interaction due to postmetamorphic tectonic events. We suggest that similar processes occurred in the Rio Nutria thrust area.

Epizonal sample 14-1 is located close to the basement-seated Río Rincon thrust and marks a distinct difference from samples originating from the less-deformed foreland-vergent imbricate thrust zone. Sample 14-1 reflects a fully reset metapelite exhumed from beneath the closure-temperature isotherm (~300 °C) originating from the hanging wall above the ramp thrust (Fig. 8C). Thus, the ages of 63 Ma (<2 µm) and 58 Ma (<0.2 µm) are interpreted as cooling ages and record a short period of thrust activity and exhumation of the hanging wall at the Río Rincon thrust in the internal domain.

Sample 14-72 is located close to the Río Nutria thrust south of the Torres del Paine intrusion. The K-Ar age of 60.8 ± 1.1 Ma in the <2 µm fraction supports our interpretation as a cooling age. The illite in the <2 µm fraction exhibits anchizonal KI values of 0.36 Δ°2Θ. Illite peak decomposition reveals a dominant PCI phase (56%) and minor WCI (36%) and I/S (8%) phases. The anchizonal KI value in the <2 µm fraction is only apparently in contradiction with the interpretation as a cooling age. The KI value is explained by the presence of retrograde illite, shifting the KI value toward poorer crystallinities. Further evidence for elevated peak metamorphic temperatures is given by the zonation of epidote and illite as well as the recrystallization of framboidal pyrite (Fig. 5D). The cooling age can be explained by thrusting associated with structural uplift along the Río Nutria thrust, which places deeper stratigraphic units of the Punta Barrosa next to the Cerro Toro Formation (Fig. 8B). Sample 14-72 originated from the hanging wall above the thrust ramp, similar to the position of sample 14-1, and it records the thrust activity of the Río Nutria thrust.

Thermal influence due to the Miocene Torres del Paine intrusive complex is considered to be unlikely, since the contact metamorphic zone is limited to a very narrow (<1.2 km) corridor surrounding the intrusion (Bodner, 2013; Süssenberger et al., 2016, 2017).

The interpretation of the <0.2 µm ages for samples within the Cerro Toro Formation (14-15, 14-21, 14-29, 14-35, 14-38, 14-46, 14-55, 14-63, and 14-75) is less evident and needs to be considered in light of the whole K-Ar database. They yielded ages between 67.1 ± 0.8 Ma and 54.5 ± 01.1 Ma, indicating a uniform postdiagenetic event of illite growth/recrystallization (Table 2; Fig. 11). KI values of this size fraction range between 0.67 and 0.30 Δ°2Θ and indicate late diagenetic to high-anchizonal conditions (Table 2). It is striking that all <0.2 µm samples from the Cerro Toro Formation but one (14-7) yielded ages of ca. 60 Ma, regardless of their stratigraphic position or geographic location.

These ages are interpreted as a weak regional thermal overprint probably related to burial metamorphism and/or a thrust-driven exhumation event. The <0.2 µm ages suggest that a widespread illite crystallization event occurred at around 60 Ma, perhaps involving orogenically driven fluids from the evolving thrust wedge in the thrust zone with maximum rock uplift. The existence of a thrusting and structural uplift event at around 60 Ma is clearly evident from samples 14-1 and 14-72, which experienced a complete reset of their <0.2 µm and <2 µm fraction ages under high-anchizonal to epizonal conditions.

(4) Early Eocene (ca. 55–46 Ma)—Illites Affected by Structural Uplift Processes

All samples of this group were obtained from the thrust zone with maximum rock uplift (Figs. 8, 11A, and 11B) and record a last period of illite recrystallization and opening of the K-Ar isotopic system between ca. 55 and 46 Ma (Fig. 10). The ages are interpreted to reflect synchronous thrusting, back thrusting, and enhanced regional rock uplift during foreland shortening in the thrust zone with maximum rock uplift. Three samples can be assigned to the Punta Barrosa Formation: 14-43, 14-71, and 14-72, <0.2 µm fraction (Fig. 11A). Samples 15-21 and 14-11 belong to the Cerro Toro Formation, sample 15-4 belongs to the Zapata Formation, and sample 15-29 belongs to the stratigraphically oldest Tobífera Formation (Fig. 11A). The samples will be individually discussed next according to their age and geographical arrangement.

The westernmost metapelitic sample 15-4 belongs to the Zapata Formation and gives ages of 47.2 ± 0.6 Ma in the <0.2 µm fraction and 53.6 ± 0.9 Ma in the <2 µm fraction (Fig. 4D; Table 2). The KI value displays distinct epizonal conditions, with 0.17 Δ°2Θ in the <2 µm fraction. The illite 10 Å reflection is a composite of a dominant WCI component (87%) and a minor PCI component (13%; Fig. 9D; Table 2). No I/S interlayering is present. The age is interpreted as a cooling age, suggesting burial temperatures above 300 °C. Since both grain-size fractions plot in a very narrow age range, they are thought to date a continuous structural uplift event beginning in early Ypresian time. The <0.2 µm age of 47.2 ± 0.6 Ma reflects the date of the neocrystallization of poorly crystallized illite on the retrograde path. Most likely, these ages are genetically linked with ages obtained for samples farther south and east (14-71, 15-29, and 15-21), suggesting an enhanced regional uplift event. However, it is difficult to resolve whether or not this structural uplift event was related to the back thrusts, as observed toward the NE, or the reactivation of the Zapata thrust, displacing the Tobífera Formation atop the Zapata Formation.

Sample 14-71, located south of the Torres del Paine intrusive complex and in the vicinity of the Río Nutria thrust, displays a cooling age of 53.3 ± 1.1 Ma in the <2 µm fraction, with a corresponding KI value of 0.28 Δ°2Θ (Table 2). Optical microscopy and XRD analyses revealed the presence of illite, albite, quartz, chlorite (chamosite), and subordinate calcite and iron oxides. Calcite is virtually absent in the <2 µm fraction and hence does not affect the K-Ar age. Photomicrographs under cross-polarized light reveal two generations of illite growth as indicated by zonation (Fig. 5C). The partial replacement and recrystallization of framboidal pyrite by euhedral, cubic pyrite crystals can be taken as an additional indication for elevated temperatures. Polytype quantification reveals the dominance of 1M illite (73%) and a minor $2M_1$ (27%) component (Table 2). Peak decomposition of the 10 Å illite reflection reveals a mixture of 55% WCI, 32% PCI, and 13% I/S interlayering (Fig. 9B; Table 2). The relatively high amount of I/S interlayering is very likely of retrograde origin and shifts the KI value toward a higher value (i.e., lower metamorphic grade). The relatively high amount of WCI, which is in contrast to many anchizonal samples of the Cerro Toro Formation, is taken as additional evidence for elevated temperatures.

Three scenarios are possible to explain the slightly younger age of this sample (53.3 ± 1.1 Ma) compared to sample 14-72 (60.8 Ma), located close by: (1) Considering that both samples are located in the hanging wall, it might indicate that thrust faulting and thrust-driven exhumation remained intermittently active over a period of at least 7 m.y. Such long-lived or reactivated thrust systems are also typical for other fold-and-thrust belt (e.g., Kirschner et al., 2003). (2) A fault-bend fold scenario associated with slightly later structural uplift of sample 14-71 would be possible and similar to the interpretation of the sample pair 15-29 and 14-1. (3) The sample might have experienced a partially reset due to a Miocene gabbro-diorite intrusion nearby. In this case, no statement about the period of thrusting could be given.

Nevertheless, the age of 53 Ma is in excellent agreement with the ages of samples 15-4 and 14-43 and corroborates the interpretation of a general thrusting/uplift event in the western part of the study area.

K-Ar fine fraction ages of sample 14-43 yielded values of 55.3 ± 1.1 Ma for the <2 µm fraction and 46.2 ± 0.6 Ma for the <0.2 µm fraction (Table 2). The ages are interpreted as cooling ages related to structural uplift from deeper stratigraphic units and local temperatures close to 300 °C. The corresponding anchizonal KI values of 0.33 Δ°2Θ in the <0.2 µm fraction and 0.31 Δ°2Θ in the <2 µm fraction are only apparently in contradiction with the cooling ages. It has to be assumed that retrograde, poorly crystallized illite grown at the end of thrusting is obscuring the true illite crystallinity established during peak metamorphic conditions. In agreement with this assumption, there is the dominant PCI component (64%) derived from peak

Figure 11 (*on following page*). (A) Geologic map of the study area with the distribution of the K-Ar data. The K-Ar data for the <0.2 µm illite fraction are indicated by open symbols, and results from the <2 µm fraction are indicated by filled symbols. K-Ar data interpreted as cooling ages are found in the thrust zone with maximum rock uplift. Sample 14-46 is located off the map to the south at the shoreline of Lago Sofia. Map is modified from Fosdick et al. (2011). Asterisk indicates age constraints for the Torres del Paine intrusive complex according to Michel et al. (2008); Fosdick et al. (2011); and Leuthold et al. (2012). (B) Results of K-Ar illite dating for different grain-size fractions: <0.2 µm (circle), <2 µm (diamond), and 2–6 µm (square). Note sample 14-1 defines the limit between the thrust zone with maximum rock uplift and the foreland-vergent imbricate thrust zone. The error bars for the K-Ar ages fall within the sample points.

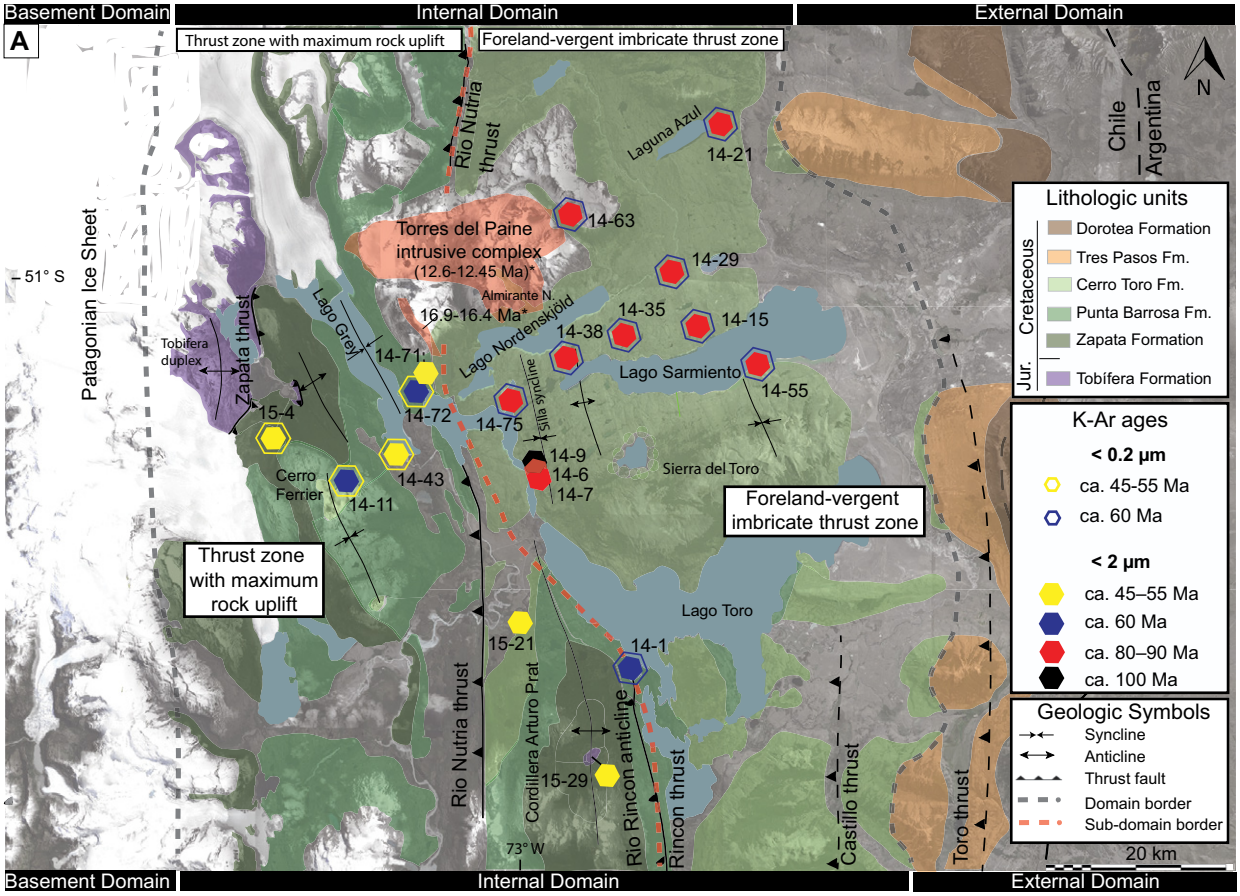
Basement Domain
Internal Domain
External Domain
A
Thrust zone with maximum rock uplift
Foreland-vergent imbricate thrust zone
Río Nutria thrust
Laguna Azul
14-21
Chile
Argentina
N
Torres del Paine intrusive complex (12.6-12.45 Ma)*
14-63
14-29
Almirante N. Nordenskjöld 16.9-16.4 Ma*
14-35
14-15
14-38
Lago Sarmiento
14-55
Lago Grey
14-71
Lago Nordenskjöld
Silla syncline
14-72
14-75
15-4
Tobífera duplex
Zapata thrust
Patagonian Ice Sheet
51° S
14-9
14-6
14-7
Sierra del Toro
Cerro Ferrier
14-43
14-11
Foreland-vergent imbricate thrust zone
Thrust zone with maximum rock uplift
Lago Toro
15-21
14-1
Río Nutria thrust
Cordillera Arturo Prat
Río Rincon anticline
15-29
Rincon thrust
Castillo thrust
Toro thrust
73° W
20 km
Lithologic units
Cretaceous
Jur.
Dorotea Formation
Tres Pasos Fm.
Cerro Toro Fm.
Punta Barrosa Fm.
Zapata Formation
Tobífera Formation
K-Ar ages
< 0.2 µm
ca. 45-55 Ma
ca. 60 Ma
< 2 µm
ca. 45–55 Ma
ca. 60 Ma
ca. 80–90 Ma
ca. 100 Ma
Geologic Symbols
Syncline
Anticline
Thrust fault
Domain border
Sub-domain border

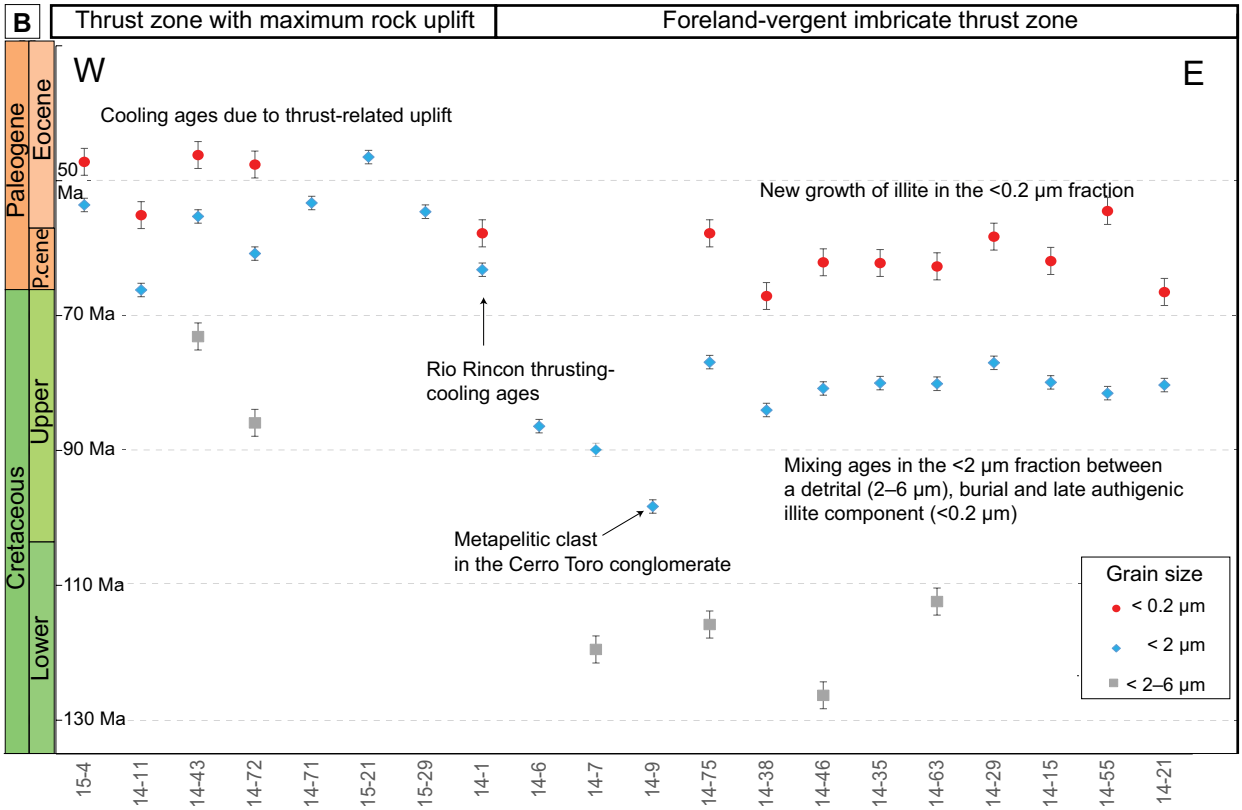
B
Thrust zone with maximum rock uplift
Foreland-vergent imbricate thrust zone
W
E
Cooling ages due to thrust-related uplift
New growth of illite in the <0.2 µm fraction
Rio Rincon thrusting-cooling ages
Mixing ages in the <2 µm fraction between a detrital (2–6 µm), burial and late authigenic illite component (<0.2 µm)
Metapelitic clast in the Cerro Toro conglomerate
Paleogene
Eocene
P.cene
Cretaceous
Upper
Lower
50 Ma
70 Ma
90 Ma
110 Ma
130 Ma
Grain size
< 0.2 µm
< 2 µm
< 2–6 µm
15-4
14-11
14-43
14-72
14-71
15-21
15-29
14-1
14-6
14-7
14-9
14-75
14-38
14-46
14-35
14-63
14-29
14-15
14-55
14-21

Figure 11.

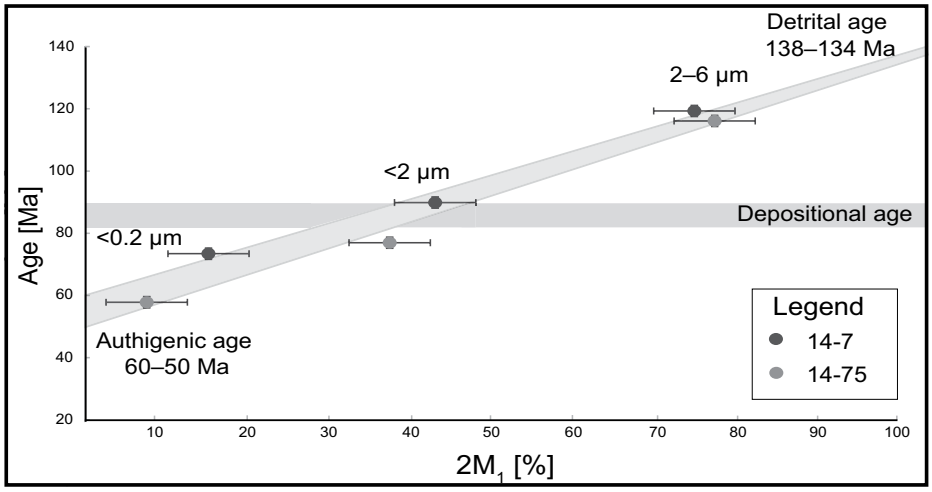

Figure 12. Results of polytype quantification yield an extrapolated authigenic age of 60–50 Ma and an extrapolated detrital age of 138–134 Ma. The range for the depositional age was defined according to age constraints in Bernhardt et al. (2012).

decomposition (Table 2). SEM imaging reveals the retrograde alteration of chlorite to chlorite/smectite mixed layering and the new growth of illite in albite pores (Fig. 6B). Sample 14-43 confirms a long-range, isochronic structural uplift event between sample 15-4 (53.6–47.2 Ma) in the west and samples 14-71 (53.3 Ma, <2 µm fraction) and 14-72 (47.6 Ma, <0.2 µm fraction) in the east (Fig. 11).

Sample 14-11 originated from the hinge zone of the Cerro Ferrier anticline and represents the sole Cerro Toro Formation outcrop west of the Río Nutria thrust. The metapelitic sample shows a typical anchizonal texture with minerals well aligned along the foliation plane (Fig. 6C). KI values indicate low-anchizonal metamorphic conditions in the <0.2 µm fraction (0.35 Δ°2Θ) and high-anchizonal conditions in the <2 µm fraction (0.29 Δ°2Θ). The proportions of $2M_1$ (20%) and $1M_d$/1M (80%) are similar to the Cerro Toro samples in the foreland-vergent imbricate thrust zone. Platy $2M_1$ illite is observed in the SEM image and represents detrital illite (Fig. 7B). The newly grown illite component replaces coarser detrital muscovite and exhibits regular smectite interstratification (Fig. 6E). The K-Ar age of 66.2 ± 1.4 Ma is slightly older than other samples in the thrust zone with maximum rock uplift and suggests a partial reset of the age during structural uplift. However, the age of the <0.2 µm fraction (55.1 ± 1 Ma) probably reflects a complete reset related to structural uplift and records the regional uplift event already observed in other samples of the thrust zone with maximum rock uplift.

Sample 15-21, located at the western limb of the Río Rincon anticline, yielded a <2 µm fraction age of 46.5 ± 5.2 Ma (Fig. 11). The KI value of 0.22 Δ°2Θ indicates lower-epizonal metamorphic conditions and suggests an interpretation as a cooling age. Optical microscopy shows newly grown illite mainly parallel to the foliation planes in the matrix. Illite peak decomposition is in agreement with the elevated temperatures and reveals a dominant WCI phase and the absence of I/S interlayering (Table 2). The $2M_1$ and 1M illite polytypes were detected with TEM (Figs. 7C and 7D). The 1M illite is interpreted as a retrograde illite phase, as peak metamorphic conditions exceeded the stability field of 1M illite. The <2 µm fraction age of 46.5 ± 5.2 Ma records structural uplift and is in good agreement with other samples of the thrust zone of maximum rock uplift.

A simplistic approach enables us to determine time-averaged exhumation rates assuming a linear geotherm (30 °C/km) and a constant cooling rate (10 °C/km). The assumption of a linear geotherm of 30 °C/km is probably valid for the mid-Eocene through early Miocene time, but it might not be valid during Eocene and late Miocene magmatism. Depths are inferred from closure temperatures assuming ~180 °C for zircon and ~300 °C for illite. Based on two time constraints—the K-Ar cooling age of 46.5 Ma (sample 15-21) and a reported zircon (U-Th)/He age of 22 Ma (Fosdick et al., 2013)—a long-term exhumation rate of 0.16 mm/yr is determined (exhumation of 4 km in 24.5 m.y.).

Sample 15-29 was collected at the contact between the metapelitic Zapata Formation and a rhyolitic body assigned to the Upper Jurassic Tobífera Formation exposed in the hinge zone of the Río Rincon anticline (Figs. 8 and 11). The rhyolitic rocks are part of the silicic volcanic unit and are described as massive, very poorly sorted lithic debris flow (Wilson, 1991; Hanson and Wilson, 1993). The mineral assemblage is dominated by quartz, albite, and chamosite as the dominant clay minerals; there is also minor illite. Newly crystallized idiomorphic titanite occurs in traces. Microcline with typical chessboard twinning is albitized. Albite porphyroblasts are embedded in a tuffaceous matrix, which is partly zoned and replaced by calcite. Occasional metapelitic clasts occur and support the assumption of a volcanic debris flow. Clay minerals occur as filling of miarolitic cavities. The filling often starts with well-crystallized illite at the rims and continues with well-crystallized chlorite (chamositic composition; Fig. 5A). Sample 15-29 gives an early Eocene age of 54.6 ± 1.4 Ma in the <2 µm fraction (Table 2). Calcite is essentially absent in the <2 µm size fraction and therefore does not affect the K-Ar system. The corresponding KI value (0.23 Δ°2Θ) indicates low-epizonal conditions (Table 2). Accordingly, the age is interpreted as a cooling age. Peak decomposition of the 10 Å illite reflection reveals the dominance of a well-crystallized illite phase (68%; Table 2). Neither illite nor chlorite shows any interstratification with smectitic phases and points to an illite crystallization at elevated temperature conditions. The age of 54.6 ± 1.4 Ma records the closing of the isotopic system related to thrust-driven exhumation.

The slightly younger age of sample 15-29 (54.6 Ma) compared to sample 14-1 (63–58 Ma), taken in the hanging wall of the Río Rincon thrust, indicates that either folding occurred immediately after thrusting or that thrusting and folding occurred simultaneously (i.e., as a fault-bend fold), followed by slightly later structural uplift along the Río Rincon anticline. Also conceivable is a genetic link to the Tenerife thrust (Fosdick et al., 2011), which is responsible for rock uplift due to structural thickening of the Zapata and Punta Barrosa Formations. The age of 54.6 ± 1.4 Ma is consistent with the time of uplift observed farther north and suggests a uniform uplift event in the thrust zone with maximum rock uplift.

Thrust-related exhumation rates can be determined assuming the aforementioned conditions (15-21) and two time constraints, the K-Ar cooling age of 54.6 Ma and a reported zircon (U-Th)/He age of 22 Ma (Fosdick et al., 2013). The calculated long-term exhumation rate of 0.12 mm/yr (exhumation of 4 km in 32.6 m.y.) is in good agreement with the calculated exhumation rate of 0.16 mm/yr for sample 15-21 and suggests a period of geological quiescence between 54 Ma and 22 Ma.

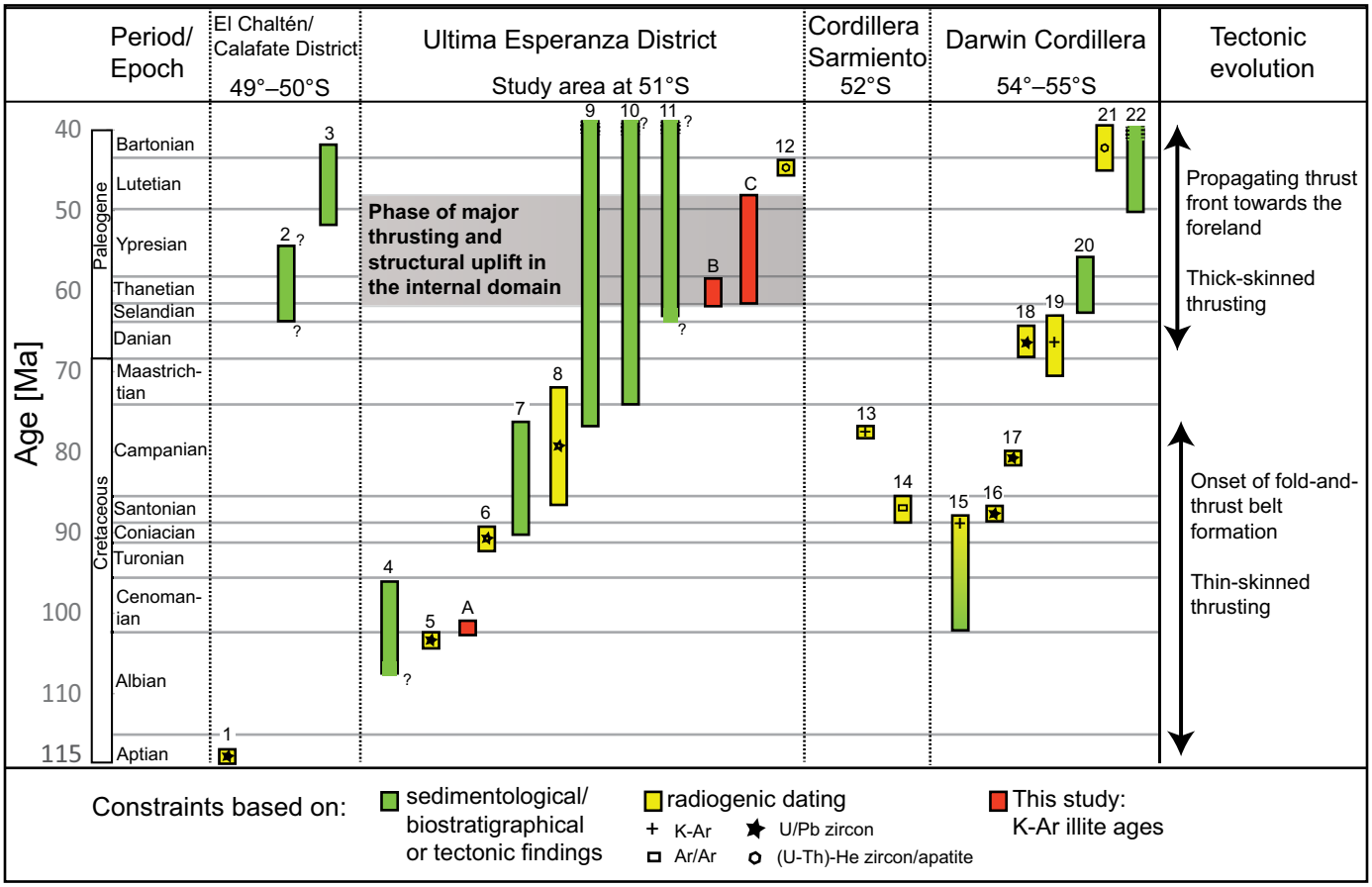

Figure 13. Compilation and correlation of known time constraints for the formation of the fold-and-thrust belt between 49°S and 55°S. K-Ar illite ages from this study are displayed as red bars, published radiogenic age data are displayed as yellow bars, and sedimentological data are displayed as green bars. (A) K-Ar age (98.3 ± 1.2 Ma, <2 µm fraction) of deformed metapelitic clast in Cerro Toro conglomerate. (B) Río Rincon thrusting between 63.2 and 57.8 Ma and Río Nutria thrusting around 60 Ma (samples 14-1, 14-72). (C) Major phase of thrusting in the internal domain between 60 and 46 Ma. (1) U/Pb zircon ages from ash beds constrain the beginning of clastic sediment deposition to 115 ± 1.9 Ma (Malkowski et al., 2015). (2) Unconformity separates marine deposits from continental Río Turbio Formation dated late Paleocene–early Eocene by Malumián and Caramés (1997) at 50°30′S–51°S. (3) Paleogene (Eocene?) compressional phase (Kraemer, 1998). (4) Compressional phase and onset of Magallanes foreland basin is signaled by the occurrence of deep-water sandstones in the Punta Barrosa Formation, dated by fossil assemblages to late Albian to Cenomanian (Cortés, 1964; Wilson, 1991). (5) U/Pb zircon crystallization age of 101 ± 1 Ma at the Zapata–Punta Barrosa transition zone indicates development of young fold-and-thrust belt (Fosdick et al., 2011). (6) Detrital U/Pb zircon ages from basal Punta Barrosa Formation record long-lasting fold-and-thrust belt activity at least until 92 Ma (Fildani et al., 2003). (7) Intense foreland subsidence and foredeep sedimentation during structural thickening and exhumation of the Tobífera thrusts, ca. 88–74 Ma (Fosdick et al., 2011). (8) U/Pb zircon dating reveals incorporation of eroded Upper Jurassic igneous rocks into the Punta Barrosa and overlying Cerro Toro Formations. Data cluster around 85–70 Ma, with maximum around 80 Ma (Romans et al., 2010; Crane and Lowe, 2008). (9) Period of thrusting defined by Fosdick et al. (2011) between 74 and 27 Ma. Lower limit defined by the displacement of the Cerro Toro Formation along the Río Nutria thrust. Upper limit defined by crosscutting relationship between Tenerife thrust and Cerro Donoso (ca. 26 Ma sensitive high-resolution ion microprobe U/Pb age; Sanchez et al., 2008). (10) Resedimented Early Cretaceous fossil fragments and palynomorphs and changes in sandstone petrofacies reflect uplift between Maastrichtian and Miocene times (Katz, 1963; Gonzalez, 1965; Macellari et al., 1989). (11) Paleogene uplift at 51°S between late Paleocene and late Eocene times (Skarmeta and Castelli, 1997). (12) Exhumation along the eastern thrust domain indicated by zircon (U-Th)/He ages between 44 and 42 Ma (Fosdick et al., 2013). (13) Whole-rock K-Ar cooling ages around 75 Ma on dikes indicate a post-tectonic metamorphic overprint (Rapalini et al., 2008). According to Fosdick et al. (2011), the enhanced regional exhumation is also responsible for Tenerife thrusting. (14) Ar/Ar ages (87–84 Ma) on syntectonic phengites (Calderón et al., 2012). (15) Deformation and metamorphism constrained by fossils in youngest deformed rocks and K-Ar biotite ages in oldest undeformed rocks to between 100 and 85 Ma (Halpern, 1973; Natland et al., 1974; Hervé et al., 1981). (16) U/Pb zircon ages reveal basin inversion and obduction prior to 86 Ma (Klepeis et al., 2010). (17) Detrital U/Pb zircon ages mark the onset of conglomerate horizons by 81–80 Ma (McAtamney et al., 2011). (18) Peak U/Pb detrital zircon populations from 66 to 62 Ma for the Fuentes and Rocallosa Formations (Mpodozis et al., 2007). (19) Beginning uplift of the Rocas Verdes block at 69–60 Ma, biotite K-Ar cooling age (Nelson, 1982). (20) San Vicente thrusting, ca. 61–55 Ma, records onset of thrust propagation (Ghiglione and Ramos, 2005). (21) Nelson (1982) established main uplift based on fission-track data between 43 and 38 Ma. (22) Río Bueno thrusting ca. 49–34 Ma (Ghiglione and Ramos, 2005).

LINKING NEW AGE DATA WITH THE KINEMATIC EVOLUTION BETWEEN 49°S AND 55°S

Onset of Patagonian Fold-and-Thrust Belt Formation

The nascent Patagonian fold-and-thrust belt was related to the inversion of the Rocas Verdes Basin, which occurred at slightly different times and with different intensities between the northernmost sector at El Chaltén (Argentina, 49°S) and the Darwin Cordillera (54°S). Several studies concluded that the shale-dominated Zapata Formation and its southern facies equivalents (i.e., Latorre Formation) acted as a major regional décollement level during the initial stage of fold-and-thrust belt formation (e.g., Fosdick et al., 2011; Betka et al., 2015). The time constraints reported here reveal fold-and-thrust belt formation proceeding from north to south, starting ~10 m.y. earlier in the Ultima Esperanza District compared to the Darwin Cordillera (54°S).

In the northernmost Argentinian sector (El Chaltén, 49°S), the onset of fold-and-thrust belt formation is constrained to 115 ± 1.9 Ma (Malkowski et al., 2015; see Fig. 13, column 1). In the Ultima Esperanza District (51°S), the onset of basin closure and fold-and-thrust belt formation occurred shortly thereafter and was first placed between late Albian and Cenomanian time by fossil assemblages and the first occurrence of deep-water sandstones at the basal Punta Barrosa Formation (Cortés, 1964; Winn and Dott, 1979; Dott et al., 1982; Wilson, 1991; Fig. 13, column 4). Zircon-U/Pb geochronology performed on volcanic ashes and detrital zircons from the Zapata–Punta Barrosa transition zone indicates thrusting between 101 ± 1 Ma (Fosdick et al., 2011; Fig. 13, column 5) and 92 ± 1 Ma (Fildani et al., 2003; Fig. 13, column 5). This study corroborates that time span based on a deformed metapelitic clast found within the Cerro Toro conglomerate, which yielded a K-Ar age of 98.3 ± 1.2 Ma in the <2 µm illite fraction (Figs. 3D, 3E, 10, and 13, column A). This age of synkinematically grown illite is interpreted to reflect a thermal event in the hinterland and records the formation of a synkinematically grown phase related to the early thrusting and uplift of the Tobífera and Zapata Formations during fold-and-thrust belt formation.

Farther south, in the Cordillera Sarmiento (52°S), syntectonic phengites from the Canal de las Montañas shear zone yielded slightly younger $^{40}Ar/^{39}Ar$ ages of ca. 85 Ma and indicate deformation and early thrusting in the basement domain (Calderón et al., 2012; Fig. 13, column 14). Based on U/Pb zircon crystallization ages, Klepeis et al. (2010) determined the initial stage of thin-skinned thrusting in the Darwin Cordillera (54°S–55°S), which placed oceanic floor of the Rocas Verdes Basin atop continental crust, prior to ca. 86 Ma (Fig. 13, column 16). Previous studies determined a broader time period of between 100 and 85 Ma for tectonic shortening and collision of the Patagonian Batholith and the South American continental margin (Halpern, 1973; Natland et al., 1974; Hervé et al., 1981; Nelson, 1982; Kohn et al., 1995; Fig. 13, column 15). The final closing of the Rocas Verdes Basin caused thrusting and imbrication of the Tobífera Formation, resulting in the so-called Tobífera duplex (e.g., Allen, 1982; Biddle et al., 1986; Wilson, 1991). Age constraints on the Tobífera duplex formation are given by whole-rock K-Ar cooling ages performed on dikes suggesting uplift at 75 Ma in the Sarmiento ophiolitic complex (51°30′S; Rapalini et al., 2008; Fig. 13, column 13). In the Ultima Esperanza District, a phase of intense foreland subsidence and foredeep sedimentation during structural thickening and exhumation of the Tobífera thrusts is constrained to ca. 88–74 Ma (Fosdick et al., 2011; Fig. 13, column 7). Additional time constraints for a matching thrust-related uplift event cluster around ca. 80 Ma and are based on the incorporation of eroded Upper Jurassic igneous rocks into the Punta Barrosa and overlying Cerro Toro Formations (Romans et al., 2010; Galaz et al., 2005; Crane and Lowe, 2008; Fig. 13, column 8). At 54°S, similar detrital zircon ages sampled in conglomerates indicate uplift and erosion of the obducted Rocas Verdes terrane and for the first time a significant detritus contribution to the foreland basin by ca. 81–80 Ma (McAtamney et al., 2011; Fig. 13, column 17).

Propagation of the Fold-and-Thrust Belt into the Internal Domain

The subsequent phase of fold-and-thrust belt formation was characterized by out-of-sequence thrusting and basement-involved thick-skinned thrusts that cut the earlier décollements and reflect the final closure of the Rocas Verdes Basin (e.g., Klepeis et al., 2010; Fosdick et al., 2011; Betka et al., 2015). In the Ultima Esperanza District (51°S), the eastward-migrating thrust front is locally documented in the Tenerife, Río Rincon, and Río Nutria thrust sheets (e.g., Wilson, 1991; Fosdick et al., 2011; Figs. 8 and 11). The first attempts to constrain the main period of foreland shortening within the internal domain were based on resedimented Lower Cretaceous fossil fragments, palynomorphs, and changes in sandstone petrofacies indicating structural uplift between the Maastrichtian and Neogene (Katz, 1963; Gonzalez, 1965; Macellari et al., 1989; Fig. 13, column 10). Skarmeta and Castelli (1997) inferred the main phase of Paleogene uplift in the area of 51°S to be between the late Paleocene and late Eocene (Fig. 13, column 11). Fosdick et al. (2011) defined a broad period of thrusting between 74 and 27 Ma, which corresponds in their kinematic evolution to "stage III—Tenerife thrusting" (Fig. 13, column 9). Other authors have argued that the Upper Paleocene to Eocene/Oligocene stratigraphic hiatus (i.e., from ca. 60 to 45 Ma) in the east-dipping frontal monocline (i.e., between the Maastrichtian Dorotea and the Eocene Río Turbio Formations; Fig. 2) may correspond to a deformational phase and uplift in the hinterland (Biddle et al., 1986; Wilson, 1991; Malumián and Caramés, 1997; Harambour, 2002; Schwartz et al., 2016). This unconformity, located immediately east of the Toro thrust, can be traced to the north (50°S–50°30′S) and is evident by displacement of the syntectonic Man Aike Formation atop the Calafate Formation (Kraemer, 1998; Malumián and Caramés, 1997; Fig. 13, column 2).

The results of illite fine fraction dating obtained in this study constrain the phase of major cooling, inferred thrusting, and structural uplift to between ca. 60 and 46 Ma (Figs. 11 and 13, column B and C) and support the idea of thrust loading in the internal domain and simultaneous uplift and erosion in the external domain (Biddle et al., 1986; Wilson, 1991; Fosdick et al., 2011). Fault and thrust activity coupled to exhumation were restricted to the frontal wedge within the thrust zone with maximum rock uplift. Tectonic thickening, folding, and uplift were slightly diachronous in different parts and mark a significant widening of the orogenic wedge. The onset of thrust and fold activity can be placed close to 60 Ma for the Río Nutria and Río Rincon thrusts (Figs. 11 and 13, column B). Farther west, deformation and structural uplift continued until ca. 46 Ma, as recorded by K-Ar cooling ages (Figs. 11 and 13, column C). The critical taper angle was probably exceeded as a result of the out-of-sequence thrusting in the internal domain. Consequently, the orogenic wedge widened, and the fold-and-thrust belt gradually migrated toward the foreland. This interpretation is in agreement with observations further south (Betka et al., 2015). Due to structural uplift and unroofing processes, the forward moving fold-and-thrust belt caused the migration of the foreland depocenter and a rapid increase in sediment supply along the monoclinal belt (Fosdick et al., 2015).

Based on basin thermal modeling, burial peak temperature conditions for the Dorotea Formation have been constrained between 164 °C and 180 °C during the early Eocene (54–46 Ma; Fosdick et al., 2015). The rapid uplift of strata due to the structural decollément below the fold-

and-thrust belt occurred slightly thereafter and is recorded by zircon (U-Th)/He ages between 44 and 42 Ma (Fosdick et al., 2013; Fig. 13, column 12). A link to the thermal overprint and uplift in the thrust zone with maximum rock uplift at ca. 46 Ma (this study) is conceivable but remains speculative due to the different closing temperatures of the various isotopic systems.

Farther south, at 54°S, Nelson (1982) established a period of moderate uplift for the Darwin Cordillera and Rocas Verdes blocks starting at ca. 69–60 Ma (Fig. 13, column 19) and a phase of accelerated uplift between 43 and 38 Ma (Fig. 13, column 21). The rapid exhumation due to basement thrusting is reflected by cooling from ~250 °C to 150 °C between 65 and 40 Ma (Kohn et al., 1995). Mpodozis et al. (2007) constrained a matching period of thrust activity near Steno Otway (53°S) between 66 and 62 Ma based on detrital U/Pb zircon populations from the Fuentes and Rocallosa Formations (i.e., southern equivalents of Tres Pasos and Dorotea Formations; Fig. 13, column 18). Ghiglione and Ramos (2005) narrowed the time of deformation further and defined two major deformation phases during the Paleocene and late Eocene: San Vicente thrusting at ca. 61–55 Ma (Fig. 13, column 20) and Río Bueno thrusting at ca. 49–34 Ma (Fig. 13, column 22). Both periods, albeit with slightly shorter activity for the later one, are also recorded by this study and suggest nearly simultaneous onset of basement-involved thrusting between 51°S and 54°S.

Farther north, at 50°S, two separate phases for the propagating thrust front have been considered in Argentina, although less well constrained (Kraemer, 1998): first, a compressional phase in the Eocene present in the western part of the fold-and-thrust belt (Fig. 13, column 3), and second, a late Miocene deformation phase present in the central and eastern part of the fold-and-thrust belt. Kraemer (1998) related the thrusting and uplift of the orogenic wedge during the Eocene with the Farallon–Aluk Ridge collision between 52 and 42 Ma (Cande and Leslie, 1986).

A late-stage deformation phase is recorded between 21 and 18 Ma along the eastern border of the internal domain, immediately at the Toro thrust (Fosdick et al., 2011). However, this late-stage deformation is not recorded by K-Ar illite dating in the studied stratigraphic units, either in the thrust zone with maximum rock uplift or in the foreland-vergent imbricate thrust zone. This is most likely due to the deeper-rooted Toro thrust fault in the Paleozoic basement complex, which left the Upper Cretaceous stratigraphic unit in the internal domain unaffected, and it provides an upper temperature on cooling (<250 °C) and inferred exhumation.

Synthesis of Fold-and-Thrust Belt Formation

The first mid- to Late Cretaceous compressional phase can be related to the collision of the Patagonian Batholith against the South American continent, causing counterclockwise movement relative to the Antarctic Peninsula while gradually closing the Rocas Verdes rift basin (e.g., Kraemer, 2003). Paleomagnetic reconstructions suggest up to 90° counterclockwise rotation in the southern Fuegian Andes (54°S –56°S), and significantly less rotation (~20%) in the northern fold-and-thrust belt (e.g., Cunningham, 1993; Maffione et al., 2010; Poblete et al., 2014). Shortening estimations from restored line-balanced cross sections suggest an increase in shortening from ~19% (Fosdick et al., 2011) in the Ultima Esperanza District (51°S) up to ~70% in Tierra del Fuego (Klepeis et al., 2010). The variation in tectonic shortening and timing of deformation along strike may be explained by the wedge-shaped Rocas Verdes Basin geometry, which widened from north to south (e.g., de Wit and Stern, 1981; Betka et al., 2015).

By the Late Cretaceous–Paleocene, the rotational movements were completed, and succeeding compressional forces were transmitted to the foreland by thick-skinned thrusting (e.g., Maffione et al., 2015). Thus, diachronous thrusting as recorded during the initiation of the fold-and-thrust belt formation was superseded by coeval Late Cretaceous–Paleocene thick-skinned tectonics along the fold-and-thrust belt. Additionally, coeval thrusting and structural uplift between 49°S and 55°S suggest constant convergence rates of the Patagonian arc against the adjacent South American continent (Fig. 13).

We propose that back thrusts and pop-up structures are important features for the out-of-sequence thrusting and exhumation in the Ultima Esperanza District. Although, back thrusts are not well recorded at the surface, their presence in the Ultima Esperanza District could be shown in seismic-reflection data and in sand analog models (Fosdick et al., 2011; Likerman et al., 2013). They are likely to have formed during the last phases of deformation around 55–45 Ma and be concentrated in the thrust zone with maximum rock uplift. Similar back thrust and pop-up structures were reported by Klepeis et al. (2010) to have contributed to the structural uplift in the Darwin Cordillera.

CONCLUSIONS

The detailed petrological study of illite and its K-Ar fine fraction ages yielded new constraints on the thermal evolution of the Magallanes foreland basin and on the timing of the Patagonian fold-and-thrust belt formation in the Ultima Esperanza District at 51°S. The thermal overprint of diagenetic, anchizonal and epizonal conditions reveals a complex pattern related to burial and thrust-driven exhumation events. Age constraints allow us to divide the internal domain of the fold-and-thrust belt into a thrust zone with maximum rock uplift and a foreland-vergent imbricate thrust zone.

The earliest indication for the onset of fold-and-thrust belt formation in the hinterland is documented in a metapelitic clast within the Upper Cretaceous Cerro Toro conglomerate, yielding a K-Ar age of ca. 98 Ma. The age records a thermal event or an episode of thrusting/uplift in the hinterland related to the presence and evolution of an emergent fold-and-thrust belt. In the foreland-vergent imbricate thrust zone, the burial conditions never attained temperatures high enough to reset the K-Ar ages. This is reflected in a homogenous pattern of mixing ages around 80 Ma. Extrapolated detrital ages inferred from $2M_1$ illite polytype quantification range between 138 and 134 Ma for samples of the Cerro Toro Formation and correspond best to reworked Zapata Formation as source rock. After a certain period of geological quiescence, an interval of thick-skinned thrusting and associated structural uplift commenced in the Ultima Esperanza District. The new geochronological data from this study constrain this event to between ca. 60 and 46 Ma. However, thrusting, folding, and uplift were slightly diachronous in different parts of the study area. The east-dipping Río Nutria and Río Rincon thrusts record the onset of thrust and fold activity, which can be placed close to 60 Ma. They also mark the Paleocene frontal thrust toward the less-deformed Magallanes foreland basin. In the thrust zone with maximum rock uplift, widespread activity of the frontal wedge with fault and thrust activity and associated rock uplift continued until 46 Ma, as recorded by K-Ar cooling ages. We propose that back thrusts and pop-up structures are important features for the out-of-sequence thrusting and exhumation in the Ultima Esperanza District. The phase of thrust loading between 60 and 46 Ma can be interpreted to be responsible for uplift and erosion along the frontal monocline, explaining the observed 15 m.y. unconformity. Time-averaged exhumation rates along the Río Rincon anticline (54.6–22 Ma) and along the Río Nutria thrust (46.5–22 Ma) suggest rather low exhumation rates of 1.6–1.2 mm/yr maximum. The low exhumation rates link back to constantly low subduction rates, resulting in a period of geological quiescence between 46.5 and 22 Ma.

ACKNOWLEDGMENTS

This project was funded by the Swiss National Science Foundation (grant no. 200021-149232 to Susanne T. Schmidt) and is part of the Ph.D. work of Annette Süssenberger. We thank Agathe Martignier for secondary electron microscope support (University of Geneva), Markus Schaffer for access to the transmission electron microscope facility at the Swiss Accident Insurance Fund (SUVA), Lucerne, Switzerland, Willem B. Stern (University of Basel) for discussion on measuring clays by X-ray diffraction, and Richard Spikings (University of Geneva) as well as Jean-Luc Epard (University of Lausanne) for fruitful discussions. We are thankful to Sam Carmalt for reviewing the English of the manuscript. The student research assistants and Sabrina Neumann of the K-Ar laboratory (University of Göttingen) are thanked for their help with sample analysis. We are grateful to the administration of CONAF (Corporación Nacional Forestal de Chile) for park access and sampling permission, as well as for local logistic support. Annette Süssenberger is thankful for the financial support of the Ernst et Lucie Schmidheiny Foundation and the August Lombard Foundation at the University of Geneva. We are grateful for the thorough and constructive review by Julie Fosdick, which broadened our understanding on the Patagonian fold-and-thrust belt. We thank Chris Hall for his review and the suggestion to include the density probability plot. We also thank the editors Brad Singer and Luca Ferrari for handling our manuscript.

REFERENCES CITED

Abad, I., 2007, Physical meaning and applications of the illite Kübler index: Measuring reaction progress in low-grade metamorphism, *in* Nieto, F., and Jiménez-Millan, J.J., eds., Diagenesis and Low-Temperature Metamorphism: Theory, Methods and Regional Aspects: Jaén, Union Grafica, Volume 3, p. 53–64.

Abad, I., Nieto, F., Peacor, D.R., and Velilla, N., 2003, Prograde and retrograde diagenetic and metamorphic evolution in metapelitic rocks of Sierra Espuna (Spain): Clay Minerals, v. 38, no. 1, p. 1–23, https://doi.org/10.1180/0009855033810074.

Ahrendt, H., Ribbert, K.H., Vanguestaine, M., and Wemmer, K., 2001, K-Ar and acritarch dating of phyllite clasts from a resedimented Middle Devonian conglomerate in the northwestern part of the Rhenish Slate Mountains: German Journal of Geology, v. 152, no. 2–4, p. 365–377, https://doi.org/10.1127/zdgg/152/2001/365.

Allen, R.B., 1982, Geologia de la Cordillera Sarmiento, Andes Patagonicos, entre los 501000 y 521150 Lat. S, Magallanes, Chile: Servicio Nacional Geologia Minería de Chile Boletin 38, 46 p.

Altenberger, U., Oberhänsli, R., Putlitz, B., and Wemmer, K., 2003, Tectonic controls and Cenozoic magmatism at the Torres del Paine, southern Andes (Chile, 51°10′S): Revista Geológica de Chile, v. 30, no. 1, p. 65–81, https://doi.org/10.4067/S0716-02082003000100005.

Bernhardt, A., Jobe, Z.R., and Lowe, D.R., 2011, Stratigraphic evolution of a submarine channel–lobe complex system in a narrow fairway within the Magallanes foreland basin, Cerro Toro Formation, southern Chile: Marine and Petroleum Geology, v. 28, no. 3, p. 785–806, https://doi.org/10.1016/j.marpetgeo.2010.05.013.

Bernhardt, A., Jobe, Z.R., Grove, M., and Lowe, D.R., 2012, Palaeogeography and diachronous infill of an ancient deep-marine foreland basin, Upper Cretaceous Cerro Toro Formation, Magallanes Basin: Basin Research, v. 24, no. 3, p. 269–294, https://doi.org/10.1111/j.1365-2117.2011.00528.x.

Betka, P., Klepeis, K., and Mosher, S., 2015, Along-strike variation in crustal shortening and kinematic evolution of the base of a retroarc fold-and-thrust belt: Magallanes, Chile 53°S–54°S: Geological Society of America Bulletin, v. 127, no. 7–8, p. 1108–1134, https://doi.org/10.1130/B31130.1.

Biddle, K.T., Uliana, M.A., Mitchum, R.M., Fitzgerald, M.G., and Wright, R.C., 1986, The stratigraphic and structural evolution of the central and eastern Magallanes Basin, South America, *in* Allen, P.A., and Homewood, P., eds., Foreland Basins: International Association of Sedimentologists Special Publication 8, p. 41–61.

Bodner, R., 2013, Metamorphism and Kinetics in the Torres del Paine Contact Aureole [Ph.D. thesis]: Lausanne, Switzerland, University of Lausanne, 164 p.

Bruhn, R.L., Stern, C.R., and de Wit, M.J., 1978, Field and geochemical data bearing on the development of a Mesozoic volcano-tectonic rift zone and back-arc basin in southernmost South America: Earth and Planetary Science Letters, v. 41, no. 1, p. 32–46, https://doi.org/10.1016/0012-821X(78)90039-0.

Calderón, M., Fildani, A., Hervé, F., Fanning, C.M., Weislogel, A., and Cordani, U., 2007, Late Jurassic bimodal magmatism in the northern sea-floor remnant of the Rocas Verdes Basin, southern Patagonian Andes: Journal of the Geological Society [London], v. 164, no. 5, p. 1011–1022, https://doi.org/10.1144/0016-76492006-102.

Calderón, M., Fosdick, J.C., Warren, C., Massonne, H.J., Fanning, C.M., Cury, L.F., Schwanethal, J., Fonseca, P.E., Galaz, G., Gaytán, D., and Hervé, F., 2012, The low-grade Canal de las Montañas shear zone and its role in the tectonic emplacement of the Sarmiento ophiolitic complex and Late Cretaceous Patagonian Andes orogeny, Chile: Tectonophysics, v. 524–525, p. 165–185, https://doi.org/10.1016/j.tecto.2011.12.034.

Cande, S.C., and Leslie, R.B., 1986, Late Cenozoic tectonics of the southern Chile Trench: Journal of Geophysical Research, v. 91, no. B1, p. 471–496, https://doi.org/10.1029/JB091iB01p00471.

Cecioni, G.O., 1957, Cretaceous flysch and molasse in Departamento Ultima Esperanza, Magallanes Province, Chile: American Association of Petroleum Geologists, v. 41, no. 3, p. 538–564.

Clauer, N., and Chaudhuri, S., 1995, Clays in Crustal Environments: Isotope Dating and Tracing: Berlin, Springer, 359 p., https://doi.org/10.1007/978-3-642-79085-0.

Cortés, R., 1964, Estratigrafía y un Estudio de Paleocomentes del Flysch Cretáceo del Depto. de Ultima Esperanza [Tesis de grado]: Santiago, Chile, Universidad Técnico del Estado, 117 p.

Covault, J.A., Romans, B.W., and Graham, S.A., 2009, Outcrop expression of a continental-margin-scale shelf-edge delta from the Cretaceous Magallanes Basin, Chile: Journal of Sedimentary Research, v. 79, no. 7, p. 523–539, https://doi.org/10.2110/jsr.2009.053.

Crane, W.H., and Lowe, D.R., 2008, Architecture and evolution of the Paine channel complex, Cerro Toro Formation (Upper Cretaceous), Silla syncline, Magallanes Basin, Chile: Sedimentology, v. 55, no. 4, p. 979–1009, https://doi.org/10.1111/j.1365-3091.2007.00933.x.

Cunningham, W.D., 1993, Strike-slip faults in the southernmost Andes and the development of the Patagonian orocline: Tectonics, v. 12, no. 1, p. 169–186, https://doi.org/10.1029/92TC01790.

Dalziel, I.W.D., 1981, Back-arc extension in the southern Andes: A review and critical reappraisal: Philosophical Transactions of the Royal Society of London, v. 300, no. 1454, p. 319–335, https://doi.org/10.1098/rsta.1981.0067.

Dalziel, I.W.D., 1986, Collision and Cordilleran orogenesis: An Andean perspective, *in* Coward, M.P., and Ries, A.C., eds., Collision Tectonics: Geological Society, London, Special Publication 19, p. 389–404, https://doi.org/10.1144/GSL.SP.1986.019.01.22.

Dalziel, I.W.D., de Wit, M., and Palmer, K., 1974, Fossil marginal basin in the southern Andes: Nature, v. 250, p. 291–294, https://doi.org/10.1038/250291a0.

de Wit, M.J., and Stern, C.R., 1981, Variations in the degree of crustal extension during formation of a back-arc basin: Tectonophysics, v. 72, p. 229–260, https://doi.org/10.1016/0040-1951(81)90240-7.

Dong, H., Hall, C.M., Peacor, D.R., and Halliday, A.N., 1995, Mechanisms of argon retention in clays revealed by laser ^{40}Ar-^{39}Ar dating: Science, v. 267, no. 5196, p. 355–359, https://doi.org/10.1126/science.267.5196.355.

Dong, H., Hall, C.M., Halliday, A.N., Peacor, D.R., Merriman, R.J., and Roberts, B., 1997, $^{40}Ar/^{39}Ar$ illite dating of late Caledonian (Acadian) metamorphism and cooling of K-bentonites and slates from the Welsh Basin, U.K.: Earth and Planetary Science Letters, v. 150, no. 3–4, p. 337–351, https://doi.org/10.1016/S0012-821X(97)00100-3.

Dong, H., Hall, C.M., Peacor, D.R., Halliday, A.N., and Pevear, D.R., 2000, Thermal $^{40}Ar/^{39}Ar$ separation of diagenetic from detrital illitic clays in Gulf Coast shales: Earth and Planetary Science Letters, v. 175, no. 3–4, p. 309–325, https://doi.org/10.1016/S0012-821X(99)00294-0.

Dott, R.H., Winn, R.D., and Smith, C.H.L., 1982, Relationship of late Mesozoic and early Cenozoic sedimentation to the tectonic evolution of the southernmost Andes and Scotia Arc, *in* Craddock, C., ed., Antarctic Geoscience: Symposium on Antarctic Geology and Geophysics, Volume 4: Madison, Wisconsin, University of Wisconsin Press, p. 193–202.

Ferreiro Mählmann, R., Bozkaya, Ö., Potel, S., Bayon, R., Šegvić, B., and Nieto, F., 2012, The pioneer work of Bernard Kübler and Martin Frey in very low-grade metamorphic terranes: Paleo-geothermal potential of variation in Kübler-index/organic matter reflectance correlations. A review: Swiss Journal of Geosciences, v. 105, no. 2, p. 121–152, https://doi.org/10.1007/s00015-012-0115-3.

Fildani, A., and Hessler, A.M., 2005, Stratigraphic record across a retroarc basin inversion: Rocas Verdes–Magallanes Basin, Patagonian Andes, Chile: Geological Society of America Bulletin, v. 117, no. 11, p. 1596–1614, https://doi.org/10.1130/B25708.1.

Fildani, A., Cope, T.D., Graham, S.A., and Wooden, J.L., 2003, Initiation of the Magallanes foreland basin: Timing of the southernmost Patagonian Andes orogeny revised by detrital zircon provenance analysis: Geology, v. 31, no. 12, p. 1081–1084, https://doi.org/10.1130/G20016.1.

Fitz-Díaz, E., Hall, C.M., and van der Pluijm, B.A., 2016, XRD-based $^{40}Ar/^{39}Ar$ age correction for fine-grained illite, with application to folded carbonates in the Monterrey salient (northern Mexico): Geochimica et Cosmochimica Acta, v. 181, p. 201–216, https://doi.org/10.1016/j.gca.2016.02.004.

Fosdick, J.C., Romans, B.W., Fildani, A., Bernhardt, A., Calderon, M., and Graham, S.A., 2011, Kinematic evolution of the Patagonian retroarc fold-and-thrust belt and Magallanes foreland basin, Chile and Argentina, 51°30′S: Geological Society of America Bulletin, v. 123, no. 9–10, p. 1679–1698, https://doi.org/10.1130/B30242.1.

Fosdick, J.C., Grove, M., Hourigan, J.K., and Calderón, M., 2013, Retroarc deformation and exhumation near the end of the Andes, southern Patagonia: Earth and Planetary Science Letters, v. 361, p. 504–517, https://doi.org/10.1016/j.epsl.2012.12.007.

Fosdick, J.C., Grove, M., Graham, S.A., Hourigan, J.K., Lovera, O., and Romans, B.W., 2015, Detrital thermochronologic record of burial heating and sediment recycling in the Magallanes foreland basin, Patagonian Andes: Basin Research, v. 27, no. 4, p. 546–572, https://doi.org/10.1111/bre.12088.

Fuenzalida, R., and Covacevich, V.C., 1988, Volcanismo y bioestratigrafia del Jurásico Superior y Cretácico Inferior en la Cordillera Patagónica, Region de Magallanes, Chile, *in* 5th Congreso Geologico Chileno, Tomo III: Santiago, Chile, Departamento de Geofisica y Geología Universidad de Chile, p. 159–183.

Galaz, G., Hervé, F., and Calderón, M., 2005, Metamorfismo y deformación de la Formación Tobífera en la cordillera Riesco, región de Magallanes, Chile: Evidencias para su evolución tectónica: Revista de la Asociación Geológica Argentina, v. 60, no. 4, p. 762–774.

García, J.-L., Hall, B.L., Kaplan, M.R., Vega, R.M., and Strelin, J.A., 2014, Glacial geomorphology of the Torres del Paine region (southern Patagonia): Implications for glaciation, deglaciation and paleolake history: Geomorphology, v. 204, p. 599–616, https://doi.org/10.1016/j.geomorph.2013.08.036.

Ghiglione, M.C., and Ramos, V.A., 2005, Progression of deformation and sedimentation in the southernmost Andes: Tectonophysics, v. 405, no. 1–4, p. 25–46, https://doi.org/10.1016/j.tecto.2005.05.004.

Ghiglione, M.C., Suarez, F., Ambrosio, A., Da Poian, G., Cristallini, E.O., Pizzio, M.F., and Reinoso, R.M., 2009, Structure and evolution of the Austral Basin fold-thrust belt, southern Patagonian Andes: Revista de la Asociación Geológica Argentina, v. 65, no. 1, p. 215–226.

Ghiglione, M.C., Likerman, J., Barberón, V., Beatriz Giambiagi, L., Aguirre-Urreta, B., and Suarez, F., 2014, Geodynamic context for the deposition of coarse-grained deep-water axial channel systems in the Patagonian Andes: Basin Research, v. 26, no. 6, p. 726–745, https://doi.org/10.1111/bre.12061.

Gonzalez, E., 1965, La cuenca petrolífera de Magallanes: Revista Minerales, v. 91, p. 1–20.

Grathoff, G.H., and Moore, D.M., 1996, Illite polytype quantification using Wildfire© calculated X-ray diffraction patterns: Clays and Clay Minerals, v. 44, no. 6, p. 835–842, https://doi.org/10.1346/CCMN.1996.0440615.

Gust, D.A., Biddle, K.T., Phelps, D.W., and Uliana, M.A., 1985, Associated Middle to Late Jurassic volcanism and extension in southern South America: Tectonophysics, v. 116, p. 223–253, https://doi.org/10.1016/0040-1951(85)90210-0.

Halpern, M., 1973, Regional geochronology of Chile south of 50° latitude: Geological Society of America Bulletin, v. 84, no. 7, p. 2407–2422, https://doi.org/10.1130/0016-7606(1973)84<2407:RGOCSO>2.0.CO;2.

Hanson, R.E., and Wilson, T.J., 1993, Large-scale rhyolite peperites (Jurassic, southern Chile): Journal of Volcanology and Geothermal Research, v. 54, no. 3–4, p. 247–264, https://doi.org/10.1016/0377-0273(93)90066-Z.

Harambour, S.M., 2002, Deep-seated thrusts in the frontal part of the Magallanes fold and thrust belt, Ultima Esperanza, Chile, *in* Haller, M.J., ed., XV Congreso Geológico Argentino (El Calafate, 2002), Geología y Recursos Naturales de Santa Cruz: El Calafate, Asociación Geológica Argentina, p. 232.

Hervé, F., Nelson, E., Kawashita, K., and Suárez, M., 1981, New isotopic ages and the timing of orogenic events in the Cordillera Darwin, southernmost Chilean Andes: Earth and Planetary Science Letters, v. 55, no. 2, p. 257–265, https://doi.org/10.1016/0012-821X(81)90105-9.

Hervé, F., Massonne, H.J., Calderón, M., and Theye, T., 2007, Metamorphic *P-T* conditions of Late Jurassic rhyolites in the Magallanes fold and thrust belt, Patagonian Andes, Chile: Journal of Iberian Geology, v. 33, no. 1, p. 5–16.

Hubbard, S.M., Romans, B.W., and Graham, S.A., 2008, Deep-water foreland basin deposits of the Cerro Toro Formation, Magallanes Basin, Chile: Architectural elements of a sinuous basin axial channel belt: Sedimentology, v. 55, no. 5, p. 1333–1359, https://doi.org/10.1111/j.1365-3091.2007.00948.x.

Hunziker, J.C., Frey, M., Clauer, N., Dallmeyer, R.D., Friedriechsen, H., Flehmig, W., Hochstrasser, K., Roggwiler, P., and Schwander, H., 1986, The evolution of illite to muscovite: Mineralogical and isotopic data from the Glarus Alps, Switzerland: Contributions to Mineralogy and Petrology, v. 92, no. 2, p. 157–180, https://doi.org/10.1007/BF00375291.

Hurst, V.J., 1985, Dehydroxylation, rehydroxylation, and stability of kaolinite: Clays and Clay Minerals, v. 33, no. 1, p. 1–14, https://doi.org/10.1346/CCMN.1985.0330101.

Katz, H.R., 1963, Revision of Cretaceous stratigraphy in Patagonian Cordillera of Ultima Esperanza, Magallanes Province, Chile: American Association of Petroleum Geologists Bulletin, v. 47, no. 3, p. 506–524.

Kirschner, D.L., Masson, H., and Cosca, M.A., 2003, An $^{40}Ar/^{39}Ar$, Rb/Sr, and stable isotope study of micas in low-grade fold-and-thrust belt: An example from the Swiss Helvetic Alps: Contributions to Mineralogy and Petrology, v. 145, no. 4, p. 460–480, https://doi.org/10.1007/s00410-003-0461-2.

Klepeis, K., Betka, P., Clarke, G., Fanning, M., Hervé, F., Rojas, L., Mpodozis, C., and Thomson, S., 2010, Continental underthrusting and obduction during the Cretaceous closure of the Rocas Verdes rift basin, Cordillera Darwin, Patagonian Andes: Tectonics, v. 29, no. 3, p. 1–24, https://doi.org/10.1029/2009TC002610.

Kohn, M.J., Spear, F.S., Harrison, T.M., and Dalziel, I.W.D., 1995, $^{40}Ar/^{39}Ar$ geochronology and *P-T-t* paths from the Cordillera Darwin metamorphic complex, Tierra del Fuego, Chile: Journal of Metamorphic Geology, v. 13, no. 2, p. 251–270, https://doi.org/10.1111/j.1525-1314.1995.tb00217.x.

Kraemer, P.E., 1998, Structure of the Patagonian Andes: Regional balanced cross section at 50°S, Argentina: International Geology Review, v. 40, no. 10, p. 896–915, https://doi.org/10.1080/00206819809465244.

Kraemer, P.E., 2003, Orogenic shortening and the origin of the Patagonian orocline (56° S. Lat): Journal of South American Earth Sciences, v. 15, no. 7, p. 731–748, https://doi.org/10.1016/S0895-9811(02)00132-3.

Kübler, B., 1964, Les argiles, indicateurs de métamorphisme: Revue de l'Institut Français du Pétrole, v. 19, no. 10, p. 1093–1112.

Kübler, B., 1967, La cristallinité de l'illite et les zones tout a fait supérieures du métamorphisme, *in* Schaer, J.P., ed., Etages Tectoniques Colloque de Neuchatel: A la Baconnière: Neuchâtel, Switzerland, Éditions de la Baçonnière, p. 105–122.

Leuthold, J., Müntener, O., Baumgartner, L.P., Putlitz, B., Ovtcharova, M., and Schaltegger, U., 2012, Time resolved construction of a bimodal laccolith (Torres del Paine, Patagonia): Earth and Planetary Science Letters, v. 325–326, p. 85–92, https://doi.org/10.1016/j.epsl.2012.01.032.

Likerman, J., Burlando, J.F., Cristallini, E.O., and Ghiglione, M.C., 2013, Along-strike structural variations in the southern Patagonian Andes: Insights from physical modeling: Tectonophysics, v. 590, p. 106–120, https://doi.org/10.1016/j.tecto.2013.01.018.

Macellari, C.E., Barrio, C.A., and Manassero, M.J., 1989, Upper Cretaceous to Paleocene depositional sequences and sandstone petrography of southwestern Patagonia (Argentina and Chile): Journal of South American Earth Sciences, v. 2, no. 3, p. 223–239, https://doi.org/10.1016/0895-9811(89)90031-X.

Maffione, M., Speranza, F., Faccenna, C., and Rossello, E., 2010, Paleomagnetic evidence for a pre–early Eocene (~50 Ma) bending of the Patagonian orocline (Tierra del Fuego, Argentina): Paleogeographic and tectonic implications: Earth and Planetary Science Letters, v. 289, no. 1–2, p. 273–286, https://doi.org/10.1016/j.epsl.2009.11.015.

Maffione, M., Hernandez-Moreno, C., Ghiglione, M.C., Speranza, F., van Hinsbergen, D.J.J., and Lodolo, E., 2015, Constraints on deformation of the Southern Andes since the Cretaceous from anisotropy of magnetic susceptibility: Tectonophysics, v. 665, p. 236–250, https://doi.org/10.1016/j.tecto.2015.10.008.

Malkowski, M.A., Sharman, G.R., Graham, S.A., and Fildani, A., 2015, Characterisation and diachronous initiation of coarse clastic deposition in the Magallanes-Austral foreland basin, Patagonian Andes: Basin Research, v. 29, no. 5, p. 298–326, https://doi.org/10.1111/bre.12150.

Malumián, N., 1999, La sedimentación en la Patagonia extraandina, *in* Caminos, R., ed., Geología Argentina: Buenos Aires, Servicio Geológico Minero Argentino, Instituto de Geología y Recursos Minerales, v. 29, no. 18, p. 557–612.

Malumián, N., and Caramés, A., 1997, Upper Campanian–Paleogene from the Rio Turbio coal measures in southern Argentina: Micropaleontology and the Paleocene/Eocene boundary: Journal of South American Earth Sciences, v. 10, no. 2, p. 189–201, https://doi.org/10.1016/S0895-9811(97)00015-1.

McAtamney, J., Klepeis, K., Mehrtens, C., Thomson, S., Betka, P., Rojas, L., and Snyder, S., 2011, Along-strike variability of back-arc basin collapse and the initiation of sedimentation in the Magallanes foreland basin, southernmost Andes (53–54.5°S): Tectonics, v. 30, TC5001, https://doi.org/10.1029/2010TC002826.

Merriman, R.J., and Frey, M., 1999, Patterns of very low-grade metamorphism in metapelitic rocks, *in* Frey, M., and Robinson, D., eds., Low-Grade Metamorphism: Oxford, UK, Blackwell Science Ltd., p. 61–107.

Merriman, R.J., Roberts, B., and Peacor, D.R., 1990, A transmission electron microscope study of white mica crystallite size distribution in a mudstone to slate transitional sequence, North Wales, UK: Contributions to Mineralogy and Petrology, v. 106, no. 1, p. 27–40, https://doi.org/10.1007/BF00306406.

Michel, J., Baumgartner, L., Putlitz, B., Schaltegger, U., and Ovtcharova, M., 2008, Incremental growth of the Patagonian Torres del Paine laccolith over 90 k.y.: Geology, v. 36, no. 6, p. 459–462, https://doi.org/10.1130/G24546A.1.

Moore, D.M., and Reynolds, R.C., Jr., 1997, X-ray Diffraction and the Identification and Analysis of Clay Minerals: Oxford, Oxford University Press, 400 p.

Mpodozis, C., Alvarez, P., Elgueta, S., Mella, P., Hervé, F., and Fanning, M., 2007, Revised Cretaceous stratigraphy of the Magallanes foreland basin at Seno Skyring: Regional implications of new SHRIMP age data on detrital zircon populations, *in* Alain Demant, ed., GEOSUR 2007 International Congress on the Geology and Geophysics of the Southern Hemisphere: Santiago, Chile, Pontificia Universidad Católica de Chile abstract, p. 106.

Natland, M.L., Gonzalez, E.P., Canon, A., and Ernst, M., 1974, A System of Stages for Correlation of Magallanes Basin sediments: Geological Society of America Memoir 139, 126 p., https://doi.org/10.1130/MEM139-p1.

Nelson, E.P., 1982, Restricted access post-tectonic uplift of the Cordillera Darwin orogenic core complex: Evidence from fission track geochronology and closing temperature–time relationships: Journal of the Geological Society [London], v. 139, no. 6, p. 755–761, https://doi.org/10.1144/gsjgs.139.6.0755.

Nieto, F., and Peacor, P.D., eds., 1993, Regional retrograde alteration of prograde pelite sequences to lower grade hydrated assemblages: TERRA Abstracts (Blackwell Publishing), v. 5, p. 419.

Pankhurst, R.J., Riley, T.R., Fanning, C.M., and Kelly, S.P., 2000, Episodic silicic volcanism in Patagonia and the Antarctic Peninsula: Chronology of magmatism associated with the break-up of Gondwana: Journal of Petrology, v. 41, no. 5, p. 605–625, https://doi.org/10.1093/petrology/41.5.605.

Perry, E.A., 1974, Diagenesis and the K-Ar dating of shales and clay minerals: Geological Society of America Bulletin, v. 85, no. 5, p. 827–830, https://doi.org/10.1130/0016-7606(1974)85<827:DATKDO>2.0.CO;2.

Pevear, D.R., 1992, Illite age analysis: A new tool for basin thermal history analysis, *in* Kharaka, Y.M., and Maest, A.S., eds., Water-Rock Interaction: Proceedings of the 7th International Symposium, Park City Utah: Rotterdam, Netherlands, Balkema, p. 1251–1254.

Pevear, D.R., 1999, Illite and hydrocarbon exploration: Proceedings of the National Academy of Sciences of the United States of America, v. 96, no. 7, p. 3440–3446, https://doi.org/10.1073/pnas.96.7.3440.

Poblete, F., Roperch, P., Hervé, F., Diraison, M., Espinoza, M., and Arriagada, C., 2014, The curved Magallanes fold and thrust belt: Tectonic insights from a paleomagnetic and anisotropy of magnetic susceptibility study: Tectonics, v. 33, no. 12, p. 2526–2551, https://doi.org/10.1002/2014TC003555.

Purdy, J.W., and Jäger, E., 1976, K-Ar ages on rock-forming minerals from the Central Alps: Memorie Instituto Geologia Mineralogia Universita Padova, v. 30, p. 1–31.

Rabinowitz, P.D., and LaBreque, J., 1979, The Mesozoic South Atlantic Ocean and evolution of its continental margins: Journal of Geophysical Research, v. 84, no. B11, p. 5973–6002, https://doi.org/10.1029/JB084iB11p05973.

Ramos, V.A., 1989, Andean Foothills structures in northern Magallanes Basin, Argentina: American Association of Petroleum Geologists Bulletin, v. 73, no. 7, p. 887–903.

Rapalini, A.E., Calderón, M., Singer, S., Hervé, F., and Cordani, U., 2008, Tectonic implications of a paleomagnetic study of the Sarmiento ophiolitic complex, southern Chile: Tectonophysics, v. 452, no. 1–4, p. 29–41, https://doi.org/10.1016/j.tecto.2008.01.005.

Rickard, D.T., 1970, The origin of framboids: Lithos, v. 3, p. 269–293, https://doi.org/10.1016/0024-4937(70)90079-4.

Romans, B.W., Hubbard, S.M., and Graham, S.A., 2009, Stratigraphic evolution of an outcropping continen-

tal slope system, Tres Pasos Formation at Cerro Divisadero, Chile: Sedimentology, v. 56, no. 3, p. 737–764, https://doi.org/10.1111/j.1365-3091.2008.00995.x.

Romans, B.W., Fildani, A., Graham, S.A., Hubbard, S.M., and Covault, J.A., 2010, Importance of predecessor basin history on sedimentary fill of a retroarc foreland basin: Provenance analysis of the Cretaceous Magallanes Basin, Chile (50–52°S): Basin Research, v. 22, no. 5, p. 640–658, https://doi.org/10.1111/j.1365-2117.2009.00443.x.

Sanchez, A., Hervé, F., and de Saint Blanquet, M., 2008, Relations between plutonism in the back-arc region in southern Patagonia and Chile Rise subduction: Nice, France, A geochronological review, *in* 7th International Symposium on Andean Geodynamics, p. 485–488.

Schwartz, T.M., Malkowski, M.A., and Graham, S.A., 2012, Evaluation of the close-out of deep-marine deposition in the Magallanes/Austral Basin, Patagonian Chile and Argentina: American Association of Petroleum Geologists Search and Discovery Article 90142: Long Beach, AAPG Annual Convention and Exhibition, 22–25 April.

Schwartz, T.M., Fosdick, J.C., and Graham, S.A., 2016, Using detrital zircon U-Pb ages to calculate Late Cretaceous sedimentation rates in the Magallanes-Austral Basin, Patagonia: Basin Research, no. 1365-2117, https://doi.org/10.1111/bre.12198.

Scott, K.M., 1966, Sedimentology and dispersal pattern of a Cretaceous flysch sequence, Patagonian Andes: Southern Chile: American Association of Petroleum Geologists Bulletin, v. 50, no. 1, p. 72–107.

Shultz, M.R., Fildani, A., Cope, T.D., and Graham, S.A., 2005, Deposition and stratigraphic architecture of an outcropping ancient slope system: Tres Pasos Formation, Magallanes Basin, southern Chile, *in* Hodgson, D.M., and Flint, S.S., eds., Submarine Slope Systems: Process and Products: Geological Society [London] Special Publication 244, p. 27–50, https://doi.org/10.1144/GSL.SP.2005.244.01.03.

Skarmeta, J.J., and Castelli, J.C., 1997, Intrusión sintectónica del Granito de las Torres del Paine, Andes Patagónicos de Chile: Revista Geológica de Chile, v. 24, no. 1, p. 55–74.

Środoń, J., and Eberl, D.D., 1984, Illite: Reviews in Mineralogy and Geochemistry, v. 13, no. 1, p. 495–544.

Środoń, J., Clauer, N., and Eberl, D.D., 2002, Interpretation of K-Ar dates of illitic clays from sedimentary rocks aided by modeling: The American Mineralogist, v. 87, no. 11–12, p. 1528–1535, https://doi.org/10.2138/am-2002-11-1202.

Stern, C.R., and de Wit, M.J., 2003, Rocas Verdes ophiolites, southernmost South America: Remnants of progressive stages of development of oceanic-type crust in a continental margin back-arc basin, *in* Dilek, Y., and Robinson, P.T., eds., Ophiolites in Earth History: Geological Society, London, Special Publication 218, p. 665–683, https://doi.org/10.1144/GSL.SP.2003.218.01.32.

Süssenberger, A., Schmidt, S., Segvic, B., and Baumgartner, L.P., 2016, Contact vs regional metamorphism in the area of Torres del Paine (southern Chile)—Combining Raman spectroscopy and clay investigations: Geological Society of America Abstracts with Programs, v. 48, no. 7, paper 27-3.

Süssenberger, A., Wemmer, K., and Schmidt, S., 2017, Monitoring the Ar retentivity of K/Ar illite fine fraction ages in the contact metamorphic aureole of the Torres del Paine intrusion (Chile), *in* 16th International Clay Conference: Granada, Spain, 17–21 July, Scientific Research Abstracts, Volume 7: Bari, Italy, Digilabs, p. 734.

Thomson, S.N., Brandon, M.T., Tomkin, J.H., Reiners, P.W., Vásquez, C., and Wilson, N.J., 2010, Glaciation as a destructive and constructive control on mountain building: Nature, v. 467, no. 7313, p. 313–317, https://doi.org/10.1038/nature09365.

Velde, B., 1965, Experimental determination of muscovite polymorph stabilities: The American Mineralogist, no. 50, p. 436–449.

Weaver, C.E., 1989, Clays, Muds, and Shales: Amsterdam, Netherlands Elsevier Science Publishers, Developments in Sedimentology 44, 818 p.

Wemmer, K., and Ahrendt, H., 1997, Comparative K-Ar and Rb-Sr age determinations of retrograde processes on rocks from the KTB deep drilling project: Geologische Rundschau, v. 86, no. S1, p. S272–S285, https://doi.org/10.1007/PL00014660.

Wilkin, R.T., and Barnes, H.L., 1997, Formation processes of framboidal pyrite: Geochimica et Cosmochimica Acta, v. 61, no. 2, p. 323–339, https://doi.org/10.1016/S0016-7037(96)00320-1.

Wilson, T.J., 1983, Stratigraphic and Structural Evolution of the Ultima Esperanza Foreland Fold-Thrust Belt, Patagonian Andes, Southern Chile [Ph.D. thesis]: New York, Columbia University, 360 p.

Wilson, T.J., 1991, Transition from back-arc to foreland basin development in the southernmost Andes: Stratigraphic record from the Ultima Esperanza District, Chile: Geological Society of America Bulletin, v. 103, p. 98–111, https://doi.org/10.1130/0016-7606(1991)103<0098:TFBATF>2.3.CO;2.

Winkler, H.G.F., 1976, Petrogenesis of Metamorphic Rocks (4th ed.): New York, Springer- Verlag, 334 p., https://doi.org/10.1007/978-3-662-22283-6.

Winn, R.D., and Dott, R.H., 1979, Deep-water fan-channel conglomerates of Late Cretaceous age, southern Chile: Sedimentology, v. 26, no. 2, p. 203–228, https://doi.org/10.1111/j.1365-3091.1979.tb00351.x.

Winslow, M.A., 1981, Mechanisms for basement shortening in the Andean foreland fold belt of southern South America, *in* McClay, K.R., and Price, N.J., eds., Thrust and Nappe Tectonics: Geological Society, London, Special Publication 9, p. 513–528, https://doi.org/10.1144/GSL.SP.1981.009.01.46.

Winslow, M.A., 1982, The structural evolution of the Magallanes Basin and neotectonics in the southernmost Andes, *in* Craddock, C., ed., Antarctic Geoscience: Symposium on Antarctic Geology and Geophysics: Madison, Wisconsin, University of Wisconsin Press, International Union of Geological Sciences Series B Volume 4, p. 143–154.

Yoder, H.S., and Eugster, H.P., 1955, Synthetic and natural muscovites: Geochimica et Cosmochimica Acta, v. 8, no. 5–6, p. 225–242, https://doi.org/10.1016/0016-7037(55)90001-6.

Zhao, G., Peacor, D.R., and McDowell, S.D., 1999, "Retrograde diagenesis" of clay minerals in the Precambrian Freda Sandstone, Wisconsin: Clays and Clay Minerals, v. 47, no. 2, p. 119–130, https://doi.org/10.1346/CCMN.1999.0470202.

Science Editor: Bradley S. Singer
Associate Editor: Luca Ferrari

Manuscript Received 6 February 2017
Revised Manuscript Received 16 August 2017
Manuscript Accepted 17 October 2017

Printed in the USA